Multiscale modelling of multizone gas phase propylene (co)polymerization reactors-A comprehensive review

Kusuma Kulajanpeng, Nida Sheibat-Othman, Wiwut Tanthapanichakoon, Timothy Mckenna

Multiscale modelling of multizone gas phase propylene (co)polymerization reactors – A comprehensive review

Kusuma Kulajanpeng[1,3], Nida Sheibat – Othman[2], Wiwut Tanthapanichakoon[3], Timothy F.L. McKenna[1]

[1]Université de Lyon, Université Claude Bernard Lyon 1, CPE Lyon, CNRS, UMR5128, Catalyse, Polymérisation, Procédés et Matériaux (CP2M), Villeurbanne, France

[2]Université de Lyon, Université Claude Bernard Lyon 1, CNRS, UMR 5007, LAGEPP, Villeurbanne, France

[3]SCG Chemicals Co., Ltd, Bangkok, Thailand

Correspondence

Timothy F.L. McKenna, Université de Lyon, Université Claude Bernard Lyon 1, CPE Lyon, CNRS, UMR5128, Catalyse, Polymérisation, Procédés et Matériaux (CP2M), Villeurbanne, France

Email: timothy.mckenna@univ-lyon1.fr

Keywords: polypropylene, propylene polymerization, gas phase catalytic polymerization reactors, multizone circulating reactors, multiscale modelling, thermodynamics

Abstracts

Catalysts and polymerization processes have evolved over the years. Such significant developments have allowed producers to broaden the range of polymer microstructure and process productivity, thereby making it possible to offer a wide range of end-use properties at a reasonably low cost. However, these advantages in catalyst performance and reactor operation require that we understand as much as possible about reactor operation in the broadest sense. In addition to the fundamental experimental study of polymer chemistry, this means that one needs to develop complete, robust process models. The present paper provides a rapid overview of recent developments in various gas phase propylene (co)polymerization reactors in use today, concentrating on multizone gas phase polypropylene reactors: i.e., multizone

circulating reactor (MZCR), fluidized bed reactor with internal circulation (FBR-IC), fluidized bed reactor with external circulation (FBR-EC), and horizontal stirred bed reactor (HSBR). We then concentrate on the advances in multiscale modelling of gas phase propylene polymerization reactors, from microscale kinetics at the active sites, to the mesoscale including physical transport and thermodynamic modelling at the single particle level and its boundary layer, up to the macroscale reactor modelling. A systematic guideline used for the selection of appropriate thermodynamic models is proposed for gas phase olefin polymerization processes. Finally, current challenges and remaining issues related with the development of mathematical multiscale modelling are addressed.

1 INTRODUCTION

Polypropylene (PP) is the second most produced polymer in the world today (after polyethylene), and is used across a variety of industries such as food packaging, healthcare and pharmaceuticals, infrastructure and construction, and automotive and electrical applications.[1–3] PP commercial grades can be grouped into three different grades:

(1) polypropylene homopolymers (HPPs) ─ constituted of mostly isotactic PP (iPP), and small amounts of atactic PP in semi-crystalline PP chains containing only propylene monomer;

(2) polypropylene random copolymers (RCPs) ─ constituted of PP comprising a small amount of ethylene or another α-olefin as a comonomer (usually up to 8 wt %) randomly distributed throughout the PP backbone; and

(3) polypropylene impact copolymers (ICPs), also known as “Heterophasic copolymers”. These are 2 phase materials comprise a matrix phase of homopolymer or random copolymer and an amorphous ethylene-propylene rubber (EPR) phase, with EPR having an ethylene content up to 40 %.[4,5]

PP is recognized as a versatile polymer due to its excellent chemical and temperature resistance, and attractive mechanical properties. According to a recent report, the global market of PP was worth USD ~75 billion in 2020 and is projected to reach USD 110 billion by 2028[2] due to the rising demand for convenient food packaging, and the integration of lightweight plastics for the automotive manufacturing.[2]

The manufacturing processes for polypropylene can be classified into three main categories according to the polymerization phases: slurry phase, bulk phase, and gas phase processes. Among these, gas phase reactors are the most widely used for industrial production as there is no solubility limit for hydrogen and comonomer(s) in the absence of a liquid around the reaction

medium, thereby allowing the production of polyolefin materials with a higher melt index (MI) and increased comonomer content.[6]

Gas phase processes for PP have evolved from single zone type reactors such as the conventional fluidized bed reactor (FBR) and vertical stirred bed reactors (VSBR) to advanced complex multizone reactor configurations, for instance, multizone circulating reactor (MZCR), fluidized bed reactor with internal circulation (FBR-IC), fluidized bed reactor with external circulation (FBR-EC), and horizontal stirred gas phase reactor (HSBR) configurations.

The HPPs or the RCPs can be produced in a single polymerization step using various configurations of gas phase or bulk phase reactors. However, the ICP production requires two or more polymerization steps, as the polymer is composed usually of a particle of iPP upon which we polymerize an elastomer, commonly a copolymer of ethylene and propylene, often referred to as EPR, although other copolymers (e.g., ethylene and 1-butene, and terpolymers) are beginning to be developed as well. In the first polymerization step, the iPP matrix polymer can be produced in either gas phase or bulk phase reactors; however, only gas phase reactors can be used to make the amorphous EPR in the subsequent steps. This is necessary to avoid dissolution of the amorphous phase of the copolymer in the liquid monomer/comonomer.[7] Therefore, the design of gas phase reactor configurations represents a key parameter to produce ICPs, with high rubber content (also called “high impact copolymers” or “hiPP”), and having desired particle morphology, particle size distribution (PSD), molecular weight distribution (MWD), copolymer composition distribution (CCD), and crystallinity, etc.[8]

Multiscale modelling is a useful approach to quantitatively predict the relationship between reactor operating conditions, reactor performance and polymer properties with the desired level of accuracy and detail.[9] The more detailed our description of each length scale in the process is, the more information we can extract about the process. However, in this case the model becomes complex and involves a larger number of parameters. Nevertheless, detailed multiscale models allow one to understand how the chemical effects (polymerization kinetics at the active sites), the physical effects (transport phenomena and thermodynamics at the particle level), and the reactor configuration influence the final product properties (i.e., product qualities, and molecular structure properties including MWD, comonomer composition, crystallinity, etc.).[9–12] A number of authors have reported the implementation of the multiscale framework in gas phase polyolefin polymerization to better understand the polymerization process behaviors. The practical applications of the multiscale modelling in the manufacturing processes are, for instance, product quality monitoring and control, existing process

improvement and optimization, process safety, process scale-up, and new product-process development.[9–11,13–19]

The purpose of the current work is to review and discuss the application of a multiscale modeling framework to gas phase propylene polymerization reactors and highlight key issues and challenges. Focus is placed on multizone gas phase catalytic polymerization reactors. The paper is organized as follows. We first present an overview of various gas phase reactors utilized in the manufacturing of PP. Subsequently, we discuss the mathematic modelling at different scales: microscale (kinetic modelling), mesoscale (single particle and thermodynamic modelling), and macroscale (reactor modelling). Furthermore, a general guideline for the selection of appropriate thermodynamic models is proposed. In the fourth section, we discuss the remaining issues, challenges, and potential solutions for future development of multiscale models. In the final section, general conclusions are highlighted.

2 GAS PHASE POLYPROPYLENE REACTORS AND PROCESSES

In this section, we will present an overview of commercial gas phase processes used for PP manufacturing. Table 1 shows an overview of multistage gas phase polymerization processes, and typical operating conditions of the current commercial PP production plants. Flow diagrams of some commercial processes used for gas phase propylene polymerization are provided in the Supporting Information.

Among the pure gas phase technologies, *UNIPOL PP* (FBR) has the largest share of installed capacity, followed by *NOVOLEN* (VSBR), *INNOVENE PP* (HSBR), and *SPHERIZONE* (MZCR). Ziegler-Natta catalysts are commonly used for all gas phase processes with or without prepolymerization step.

The hybrid or mixed-phase processes, in other words the combination of bulk and gas phase reactors, are able to provide a full range of products, but higher capital investment is required. For example, the *SPHERIPOL* process by LyondellBasell uses two or more loop (bulk phase) reactors for iPP, followed by one or more FBRs in series for elastomeric or highly amorphous material. In this review, we will limit the discussion to the different gas phase reactor types, not the whole processes.

Gas phase reactors for propylene (co)polymerizations (Table 2) can be simply grouped into two broad categories: single-volume and multi-volume reactors. A reactor can be qualified as a multizone reactor if it has (1) more than one physically connected reactor volumes (or zones, sections, or compartments), or (2) the ability to independently create different reaction conditions. This classification will be adopted in this review.

- The single-volume gas phase reactor: is defined as a reactor that can be approximated by one physical reaction volume (or section, zone, compartment), in which the temperature and gas concentrations (i.e., monomer, comonomer(s), chain transfer agent (hydrogen), etc.) are intended to be approximately uniform. This is the case, for example, of FBR and VSBR, as the residence time distribution (RTD) of the polymer phase in these reactors approaches that of a CSTR, providing a broad RTD.[20] Indeed, while in reality there are temperature gradients in a parts of these reactors (usually at the gas phase inlet), we cannot independently modify the conditions in each volume portion. In such reactors, it is required to have two or more reaction volumes in series to create significantly different gas compositions in each stage, in order to produce multiple different types of polymer properties (i.e., polymer molecular weight, comonomer composition, etc.) (Figure 1a). However, it is well-known that the particle structure of the product obtained from the two-stage CSTR in series can be inhomogeneous because of the residence time distribution of the reactors themselves.

- The multi-volume gas phase reactor (e.g., HSBR, and MZCR): is defined as a single reactor constituted of two or more reaction volumes interconnected in which each reaction volume can be operated (fairly) independently. It is assumed that the operating conditions (i.e. gas concentrations, feed flow rate, temperature) can be modified independently to create different reaction environments in each reaction zone, so as to have different fluid dynamic regimes, reaction temperatures, and H_2/comonomer(s) composition, thus producing different molecular weights, densities or compositions of the polymer.

An example of a multi-volume reactor is the MZCR (Figure 1b). In simple terms it can be described as two plug flow reactors (PFRs) that are independently operated under different conditions. This two-zone reactor will be presented in more detail below. A low molecular weight polymer is typically made in the first reaction volume by injecting some H_2 in the gas feed stream ─ usually the concentration of H_2 is 2-4 orders of magnitude higher than that in the second reaction volume; thus this reactor type is capable of producing bimodal molecular weight product of polyolefin in a single reactor. An illustration of the homogenous polymer structure that can be made in a two-volume reactor is also shown in the figure 1**FIGURE 1**b. In the MZCR, the growing polymer particle is continuously circulating between the two interconnecting reaction volumes with a very short residence time per pass (solid particles passing between 50 and 100 times before exiting) to generate thin polymer layers with different polymer chain compositions and different molecular weights (the so-called multi-onion-like structure), thereby enhancing homogeneity of the polymer.[21] The shorter the residence time of the successive paths between both reaction volumes, the thinner the shell (or layer).[21] These

novel features offer the possibility to produce advanced polymer structures and properties, having intimately mixed polymer compositions at the molecular level that cannot be achieved in a single-volume reactor type, post-reactor chemical modification nor by mechanical blending of the different polymers in an extruder.

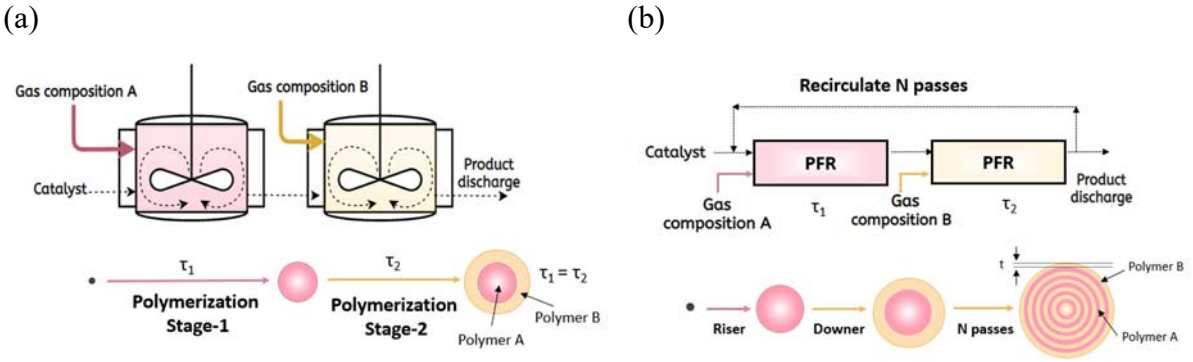

FIGURE 1 Comparison of the expected particle morphology and microstructure obtained from (a) a two-stage polymerization of 2 single-volume reactors in series, and (b) a multi-volume reactor (MZCR), adapted from Galli and Vecellio,[21] and Liu et al.[22]

2.1 Single-volume gas phase polypropylene reactors

2.1.1 Fluidized bed reactors (FBR)

The FBR consists of an empty vertical cylinder with a disengagement zone (an expanded dome vessel to reduce the rising gas velocity and the entrainment of polymer particles) (Figure 2). The flow rate of the circulating gases (including monomer, inert, chain transfer agent (CTA), and comonomer(s) for RCP production) is set to fluidize the growing polymer particles, and maintain a stable reactor temperature (by evacuating the heat of polymerization). The gas exiting the reactor is subsequently compressed, cooled and recycled back, together with make-up monomer/comonomer(s) and appropriate quantities of fresh hydrogen, to the bottom of reactor. Catalyst particles (i.e., Ziegler-Natta or metallocene catalyst) on the size order of 20–80 μm in diameter, or prepolymerized catalyst particles (around 500 μm in diameter), are continuously introduced into the FBR at a point slightly above the gas distributor to catalyze the reaction with the circulating gases. The obtained polymer is continuously withdrawn from the reactor at a point close to the bottom of the bed. Generally, a broad size distribution of polymer particles is obtained, ranging between 100–5000 μm.[8]

TABLE 1 Industrial gas phase technologies for polypropylene production.[8,20,23]

Technology	**Developer/ Owner**	**Cat. type**	**Multistage gas-phase processes**		**Operating conditions**[23]				
			Homopolymer (iPP)	**Impact copolymer (EPR)**	**P (bar)**	**T (◦C)**	**RT (hr per reactor)**	**C_2 content (% wt)**	**EPR content (% wt)**
UNIPOL	Union Carbide/ Dow Chemical	ZN	1 FBR (Condensed gas phase)	1 FBR (Gas)	25 - 35	60 - 70	~ 1	up to 19	~ 37
SUMITOMO	Sumitomo Chemical	ZN	1 FBR (Condensed gas phase)	1 FBR (Gas)	30 - 35	70 - 80	~ 1	-	-
CATALLOY	LyondellBasell	ZN	1 FBR (Condensed gas phase)	2 FBR (Gas)	20 - 40	60 - 90	~ 0.5-2	-	Up to 65
NOVOLEN	BASF/ Lummus Novolen Tech	ZN and M	1 VSBR (Gas)	1 VSBR (Non-condensed gas phase)	20 - 35	50 - 105	~ 1	up to 22	~ 43
INNOVENE	Amoco and Chisso/ Ineos	ZN and M	1 HSBR (Condensed gas phase)	1 HSBR (Gas)	22 - 30	60 - 85	~ 1	22	-
HORIZONE	Amoco and Chisso/JPP (Japan PP Corp.)	ZN and M	1 HSBR (Condensed gas phase)	1 HSBR (Gas)	25 - 30	65 - 85	~ 1	-	Up to 60
SPHERIZONE	LyondellBasell	ZN and M	1 MZCR (Gas)	1-2 FBR (Gas)	25 - 30	70 - 90	~ 1	Up to 8	-

TABLE 2 Gas phase reactor technology classified based on the number of zones (volumes) of the reactors.[8,23,24]

Volume of reactors	**Technology**	**reactor type**	**Number of zones**	**Estimation of RTD in each reactor**	**Estimation of overall RTD**	**Overall RTD distribution**	**Polymer composition distribution**
Single-volume reactors	*UNIPOL, SUMITOMO, CATALLOY*	FBR	1	1 CSTR		Broad	Broad
	NOVOLEN	VSBR	1	1 CSTR		Broad	Broad
Multi-volume reactors	*INNOVENE, HORIZONE*	HSBR	3-5	3-5 CSTRs in series	PFR	Narrow	Narrow
	SPHERIZONE	MZCR	2	2 PFRs in loop (Riser/Downer)	CSTR	Broad	Narrow
	-	FBR-IC	~2	1 CSTR (Cone) 2 PFRs in loop (Riser/Downer)	CSTR	Broad	Narrow
	-	FBR-EC	3	1 CSTR (FBR) 2 PFRs in loop (Riser/Downer)	CSTR	Broad	Narrow

Although there is a complex, recirculating flow structure in the powder phase of a CSTR (Figure 2a), it is a common practice to assume that the recirculation rate is fast enough that we can approximate the RTD of the particle phase in the FBR by that of a CSTR, which means assuming perfect mixing (i.e. assuming uniform concentrations and temperature) as suggested in Figure 2b.[6] To model a more complex RTD, we can conceptually divide the rector into interconnected zones which will allow us to better account for thermal and concentration gradients in the reactor (Figure 2c),[19,25–27] but the overall RTD of the particle powder may still be approximately that of a CSTR.

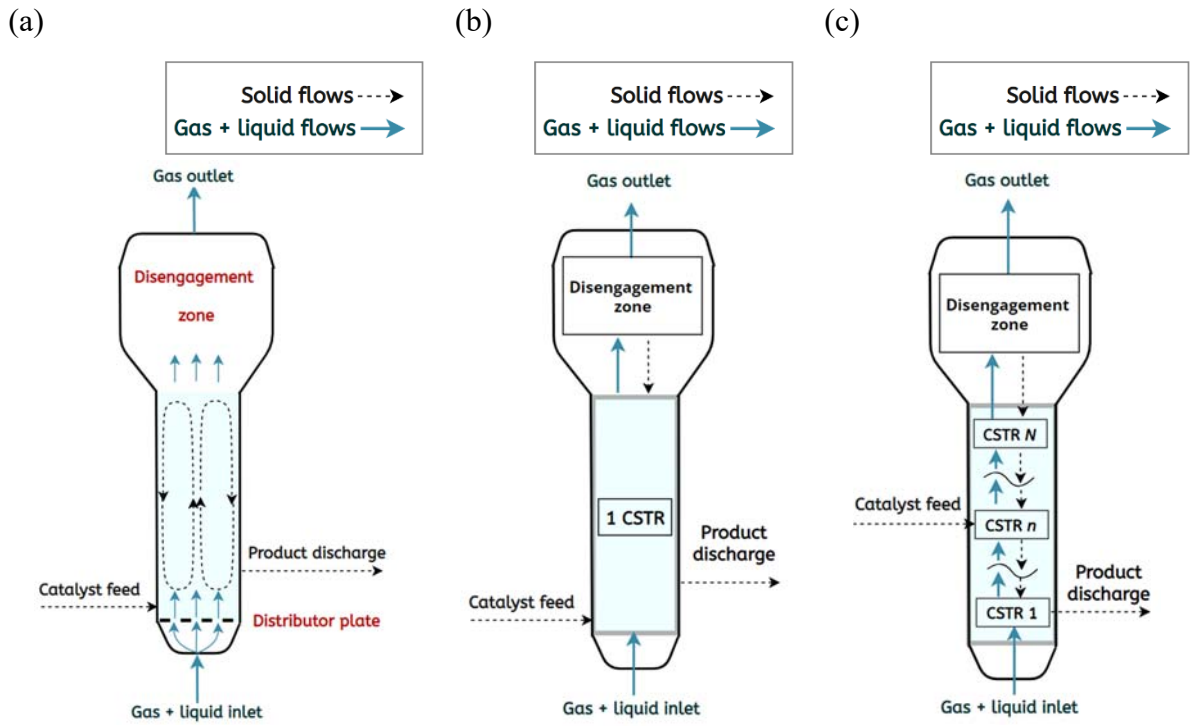

FIGURE 2 (a) Simplified diagram of a typical FBR; (b) a basic simplified FBR model as a CSTR; (c) a compartmentalized FBR model, adapted from Alves and McKenna[28]

FBRs are nowadays the dominant gas phase process for linear low-density polyethylene (LLDPE) production, and are widely used for PP production (especially ICPs), because of their high capability for heat evacuation compared to other gas phase reactors. However, since FBRs are characterized by a relatively broad RTD, the obtained product is not uniform. Indeed, a single FBR (like a single CSTR) will make polymer with a broader PSD or MWD than will a series of reactors or reaction zones. In addition, it is impossible to make polymers with complex properties (i.e., onion-like structure) using a single FBR. In these cases, it is required to have at

least two FBRs in series, to have different polymerization conditions in each reactor (i.e. temperature and gas compositions). For example, *CATALLOY* technology (see Figure 1S in Supporting Information) employs up to three FBRs in series; one for making iPP or RCPs in the first polymerization step, and two or more FBRs to produce RCP or ICPs in the second copolymerization step.

2.1.2 Vertical stirred bed reactors (VSBR)

The VSBR configuration is generally a stirred autoclave reactor with a spiral stirrer mounted at the bottom of the stirred vessel (Figure 3).[20] The agitation system is designed to keep the bed moving up along the side walls while allowing the polymer powder to move downward through the center of the bed under the influence of gravity and increasing weight of the growing polymer particles.[20] The mixture of particle powder and carrier gases is discharged from the reactor top via a dip tube. Thorough distribution of catalyst, cocatalyst, and (partially) liquified monomers at the feed point to the reactor must be achieved to avoid local overheating which would lead to the formation of agglomerates in the polymer bed. In addition, the temperature in the reactor must be controlled above the dew point of the recirculating gas to prevent condensation and pooling of liquid propylene at the bottom of the reactor which may cause uncontrolled polymerization, particle agglomerations, lump formation and fouling issues.[20] Otherwise, like the FBR, the RTD of the particles in a VSBR approaches that of a CSTR. Therefore, the VSBR is classified as a single-volume reactor. Once again, the limitation of the VSBR is recognized as the same as the FBR: the non-homogeneity of the final products due to the imposed polymer RTD, and the reduced flexibility to control polymer structures and properties. The *NOVOLEN* process is an example of the commercial process based on VSBR configuration (see Figure 2S in Supporting Information).

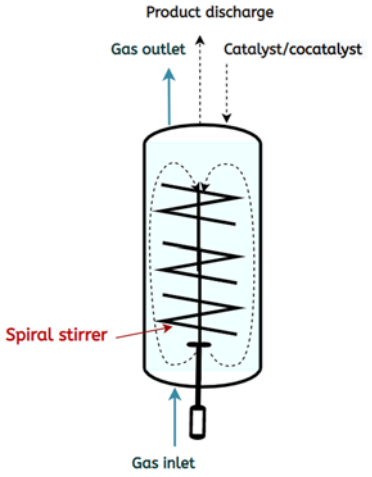

FIGURE 3 Simplified diagram of a typical vertical stirred bed reactor (VSBR)

2.2 Multi-volume gas phase polypropylene reactors

2.2.1 Multizone circulating reactor (MZCR)

The design of a multizone circulating reactor (MZCR) for polypropylene production was originally developed by LyondellBasell, and was successfully commercialized at Basell's plant in Brindisi (Italy) in the early 2000s as the basis of the *SPHERIZON*E technology.[29,30] The MZCR configuration is shown in Figure 4. The MZCR can be optionally connected with a FBR in series for the production of high impact PP, as shown in Figure 3S in the Supporting Information.[31]

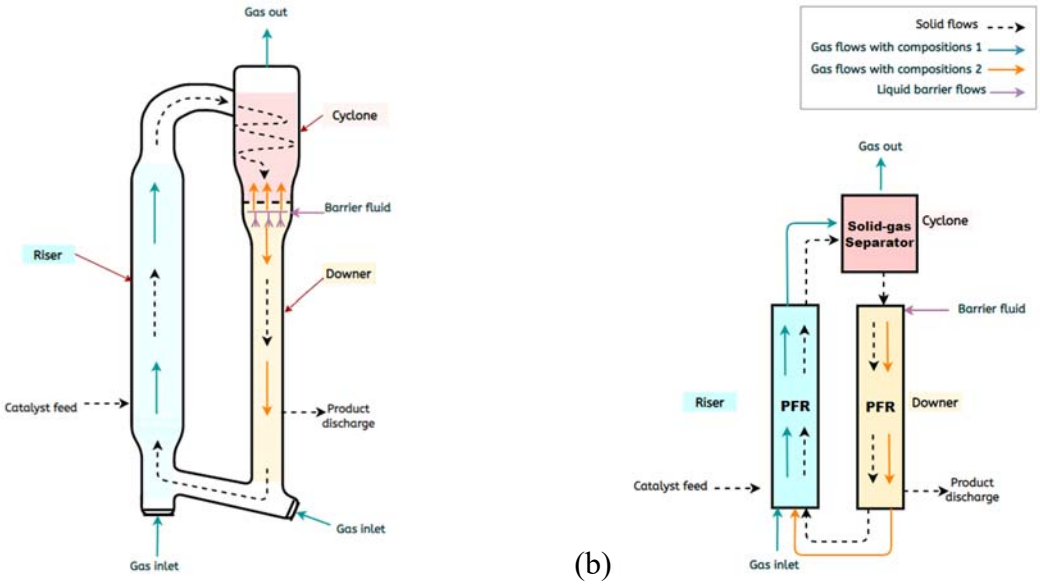

FIGURE 4 (a) Simplified diagram of MZCR, adapted from Covezzi and Mei,[29] (b) Multi-volume reactors of MZCR modeled as 2 PFRs

The MZCR consists of two interconnecting reaction volumes, the "riser" and the "downer", and a cyclone located at the top of the downer.

- Riser: In the riser, the growing particles and reacting gases move upward under fast fluidization conditions with an RTD that can be approximated by a PFR. The superficial velocity of the gas is maintained at much higher values than the terminal velocity of the particles to ensure highly and a uniform temperature along the riser.[20] The gas mixture of the riser contains a higher fraction of hydrogen than the downer, which leads to the production of a lower polymer molecular weight.
- Cyclone: A mixture of the growing particles and the remaining gases leaving the top of the riser is fed to a cyclone. In the cyclone, the polymer particles move downward by the action of gravity, and enter the downer (i.e. the second polymerization volume), while the gas is removed at the cyclone top, and is then compressed, cooled and recycled to the riser feed stream.
- Barrier fluid: Another important section of the MZCR is the barrier fluid. It is defined as the gas-liquid mixture which is introduced at the top of the downer (just below the cyclone, at the inlet of the downer) and is essentially dispersed uniformly over the upper surface of the densified polymer particles. Once it enters the downer, the barrier fluid is partially evaporated to establish a net gas flow upward in the upper portion of the downer. By this way, the riser gas coming into the downer is nearly totally replaced by the evaporated gases. The gas composition of the barrier fluid is generally different from the gaseous mixture coming from the riser. In principle, this allows one to operate the reactor with different concentrations of monomer, comonomer, and hydrogen (molecular weight regulator in the riser and in the downer.). The evaporation of the barrier fluid not only acts as a barrier to the gas coming from the riser, but also helps removing the heat of reaction developed in the downer,[30] thus allowing to control the temperature profile in the downer in a reliable way.[32]
- Downer: In the downer, the growing polymer particles move downward in a plug flow mode (in a moving packed/densified form). The downer operates under conditions close to adiabatic conditions. A large part of the particles leaving the downer is recirculated to

the first polymerization volume (riser) with high recycle ratios. According to Ergun's law of moving packed bed, gas and solid in the downer co-currently flow downward, and the pressure decreases from the top to the bottom.[29,30] Since the gas phase has a different composition in the downer compared to the riser, a polymer with a different composition from that made in the riser (and thus properties) is produced here. This means that polymers with a much wider range of properties can be made in this single multizone reactor than in a single volume reactor.

A continuous circulation of the polymer particles is maintained by balancing the pressure between the two polymerization zones and by the head losses.[32] While the flow patterns of particles in both the riser and the downer are similar to plug flow conditions, the gas and particles recycling imply that the overall MZCR can be approximated by an ideal CSTR. The particles move around through the two different reaction zones between 50 and 100 times due to the influence of the high recirculation rate of the polymer particles between the two reaction volumes (about 250 to 700 ton/hr). The particle's residence time per pass is approximately 120 seconds for a full circulation cycle, whereas the overall residence time of the MZCR is roughly 2 hours. This configuration creates multiple polymerization stages, thus building up polymer layers with slightly different composition in each cycle.[8]

The holdup and residence time in each leg of the reactor can be adjusted to vary the polymer properties between the two polymerization zones to suit different requirements.[30] LyondellBasell claimed that this technology can be used to produce nearly uniform homopolymers, ranging from narrow to very broad molecular weight distributions, random copolymers or terpolymers with a better balance of stiffness and impact strength properties, including twin random copolymers as well as random and heterophasic copolymers.[31]

Heat removal is achieved either by operating the transport gas in condensed mode, or with a cooling jacket placed around the external wall of the riser and the downer tube.[20]

2.2.2 Fluidized bed reactor with internal circulation (FBR-IC)

The FBR with internal circulation (FBR-IC, Figure 5) has been designed to increase the PP production rate by an improved solid-gas mixing.[33] In this technology, the conventional FBR is divided into two compartments by installing a vertical draft tube in the center of the reactor bed (also known as "FBR with a draft tube"). As a result, the two reactor zones can be operated in two different flow regimes (one flow regime is inside the draft tube and another in

the annular region) making them different in thermal transport properties, temperature gradients and possibly even composition.[34–36]

The internal region of the draft tube forms fast fluidization state in which the growing particles and reacting gas move upward, then they are forced to make an internal circulation in the second zone of the fluidized bed (due to the disengagement zone and the reduction in velocity). The outside of the draft tube becomes an annular region in which the growing particles move downward in a densified form under the action of gravity (the so-called ‘‘moving bed’’).[36] Polymer particles leaving the bottom of the annulus region go to a conical bottom section, and are then reintroduced into the draft tube. Some polymer is discharged from the annular region near the bottom of the FBR. The flow regimes in both compartments are comparable to plug-flow conditions whereas the cone section can be considered as a CSTR (Figure 5b).[34]

According to WO Patent 00/69552[37] and US patent 2016/0002376 A1,[36] the use of the FBR with a draft tube operated in condensed mode allows us to increase the amount of condensed liquid that can be supplied in proportion to the total amount of gas feed, compared to the traditional FBR. This increases the heat removal capacity of the reactor, thus allowing a higher polymer production rate at the same reactor dimensions.

This special design is suitable for retrofitting existing FBR with a simple modification and presents several advantages over conventional FBRs as discussed above. The author of WO Patent 00/69552[37] claimed that this configuration does not offer the possibility to produce different types of polymeric chains in the different zones since the gas composition is essentially the same in both compartments during the total residence time of the particle in the reactor.[37]

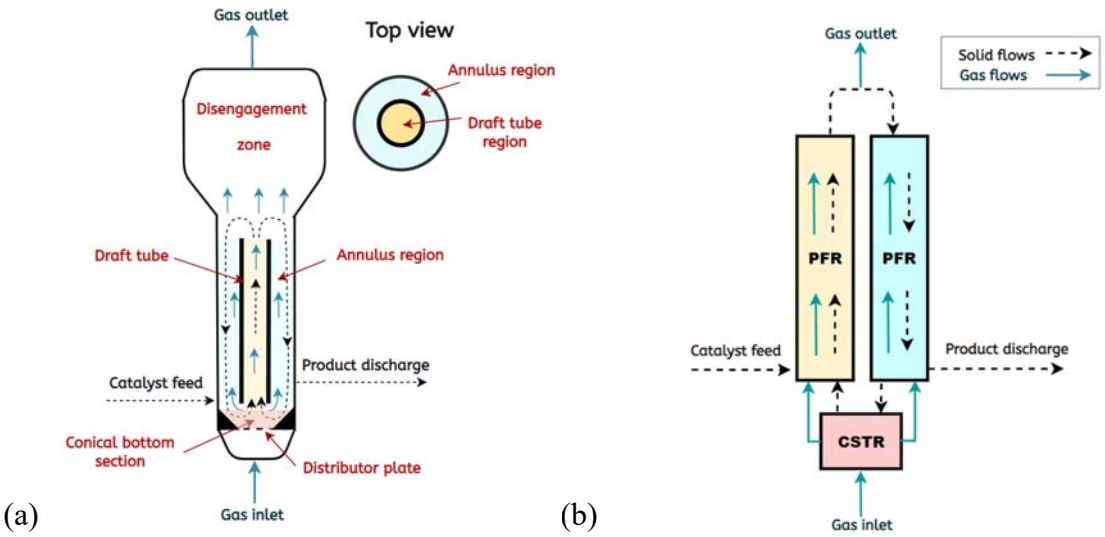

FIGURE 5 (a) Simplified diagram of fluidized bed gas phase reactor with internal circulation (FBR-IC) or FBR with a draft tube; (b) Multi-volume reactors of FBR-IC approximated by a CSTR and 2 PFRs, adapted from WO Patent 00/69552[37] and Meier et al.[34]

2.2.3 Fluidized bed reactor with external circulation (FBR-EC)

The FBR with external circulation (FBR-EC) was proposed by Basell in early 2000. This reactor extends the concept of multizone circulating reactor (Basell's *SPHERIZONE* process) in which the standard FBR is set up with three interconnected reaction volumes (Figure 6). An interconnected dip tube is added to the center of the FBR (in a comparable way as in the FBR-IC presented previously) but this tube is extended to exit the FBR and form a recycling tube. According to WO patent 2004/033505 A1,[31] the purpose of this development is to be able to retrofit the conventional FBR so as to increase the broadening the polymer MWD while maintaining a high homogeneity level of the final product. As with the internally circulating FBR, the overall effect of this configuration is to have 2 main volumes like in the MZCR. The distinction between the zones is probably not as fine or well controlled as in the MZCR (e.g. no inter-stage degassing).

The monomer gas is introduced through a distribution plate. The growing polymer particles move upward in the annular region at gas velocities above the minimum fluidization velocity. This constitutes the first reaction volume. At the top of the FBR, the particles reduce of velocity in the disengagement zone and fall back, with some of them entering the second polymerization volume (the so-called downer), the vertical pipe inserted in the center of the FBR.

In the downer, the growing polymer particles move downward in a densified form under the action of gravity, a positive gain in pressure can be obtained along the flow direction. The gas mixture present in the first zone can be partially prevented from entering the second zone by introducing a barrier fluid having different composition via lines placed at the upper part of the second reaction volume. The gas barrier mixture and the polymer particles flow downward along the second reaction volume.

The third reaction volume (the so-called riser) consists of a pipe placed externally to the FBR operated under fast fluidization to transport polymer particles exiting the bottom of the downer (i.e. the second volume) upward and reintroduce them into the first reaction volume. Similarly, the gas mixture flowing downward along the second reaction volume can be partially prevented from entering the third polymerization volume. This can be achieved by feeding a

barrier fluid at the bottom of the second polymerization volume. The polymer product is discharged from the reactor near the bottoms of the first and second polymerization zones.

Like the MZCR, this reactor configuration can be operated at different gas compositions in a single reactor allowing broadening of the MWD and CCD while maintaining a good homogeneity of the polymer particles. The flow behavior inside the riser and the downer can be described by a PFR while the annulus-shaped FBR can be considered as a CSTR.

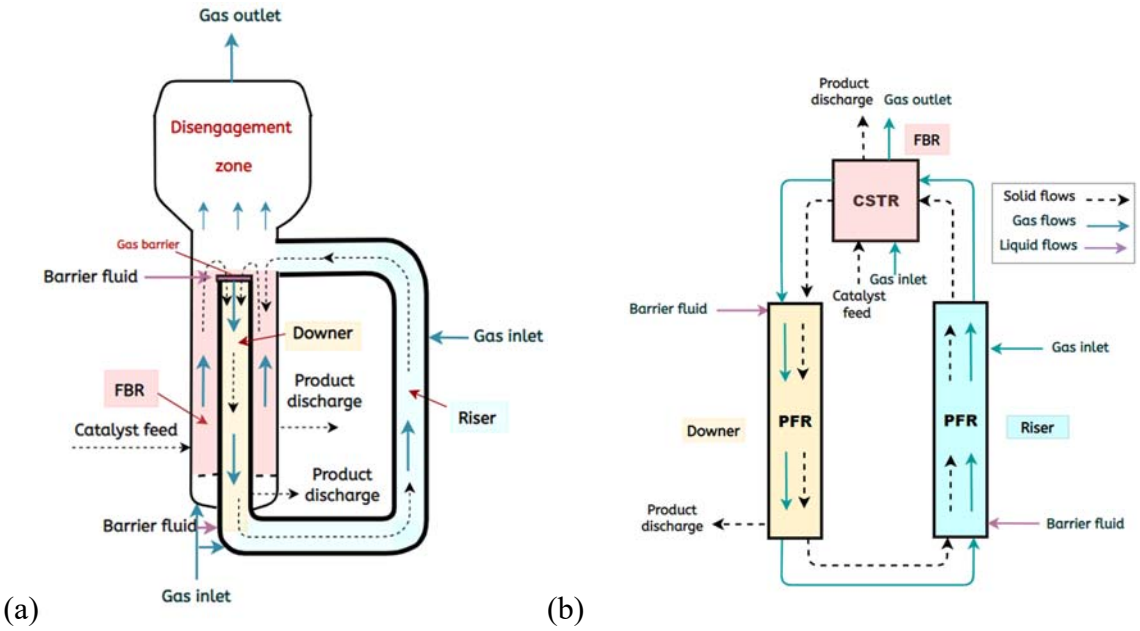

FIGURE 6 (a) Simplified diagram of a fluidized bed gas phase reactor with external circulation (FBR-EC); (b) Multi-volume reactors of FBR-EC approximated as a CSTR and 2 PFRs adapted from WO patent 2004/033505 A1[31]

2.2.4 Horizontal stirred bed reactors (HSBR)

The horizontal stirred bed reactor (HSBR) was originally developed in the 1970s for polyethylene, but is now exclusively used for PP (Figure 7a). The *INNOVENE* process based on two HSBR in series is presented in Figure 4S (see the Supporting Information). The HSBR is a horizontal cylindrical vessel mechanically stirred by paddles, mounted on a central shaft, to permit agitation of the powder. The gas phase is in cross flow with respect to the main direction of powder flow. It can be imagined as being divided into several reaction volumes that offer the ability to individually control reaction temperature, gas-phase composition and quench liquid flow rates along the axial direction of the reactor. So, a polymerizing particle can see different gas compositions, and eventually temperatures inside the single reactor. This means that one could make a polymer with a bimodal molecular weight by independently

controlling the hydrogen concentrations at the different polymerization volumes of a single HSBR, or a gradient in RCP/ICP composition by doing the same thing with a mixture of monomers.[22,38]

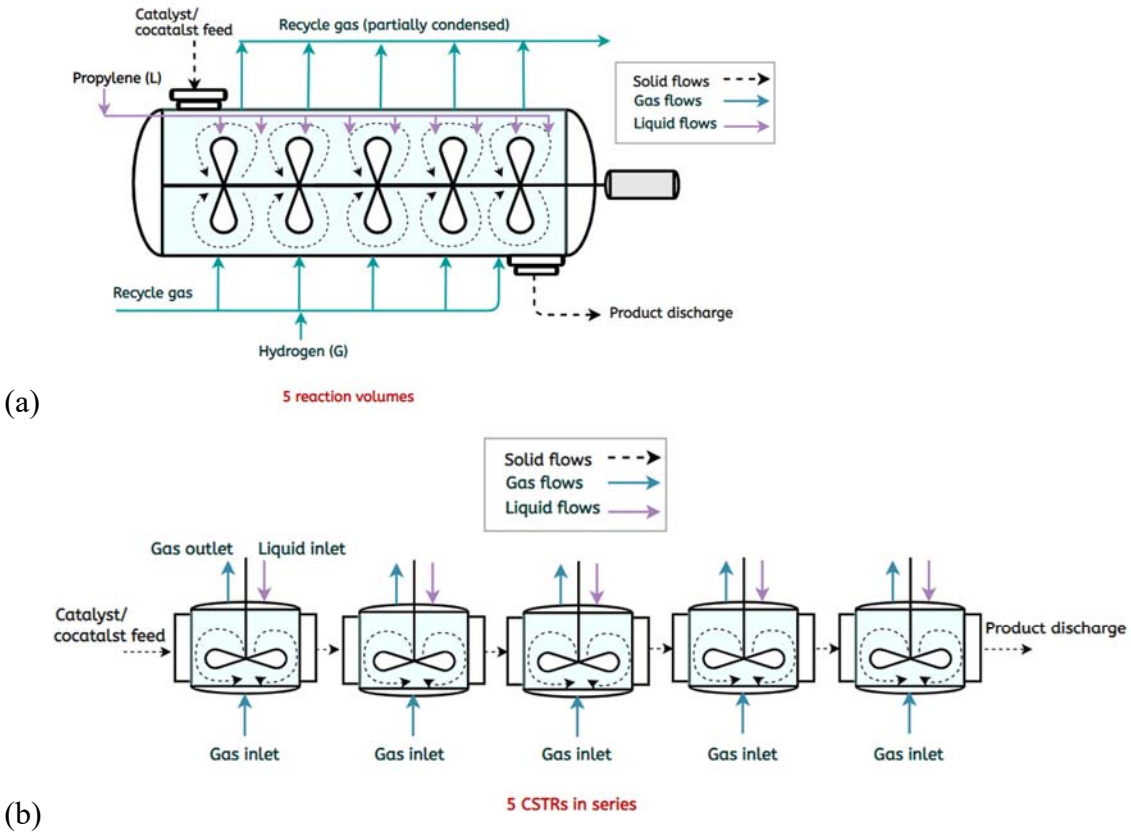

FIGURE 7 (a) Simplified diagram of a typical horizontal stirred bed reactor; (b) multi-volume reactors modelled as a 5 CSTRs in series adapted from Soares and McKenna[20]

The flow pattern of the powder and the RTD inside of the HSBR are unique and differ from other gas phase reactors. Indeed, in the HSBR, the polymer RTD is narrower compared to single-volume gas phase reactors (e.g. FBR, and VSBR). The polymer RTD of the HSBR is roughly comparable to a PFR[20] and can be described roughly by three to five equi-volume CSTRs in series depending on the size of the reactor[38] (see Figure 7b). However, more sophisticated powder RTD have also been proposed, where the CSTRs in Figure 7b can be thought of as having different sizes, with eventually back mixing of the powder between zones.[39]

3 MATHEMATICAL MODELLING OF MULTIZONE GAS PHASE (CO)POLYPROPYLENE REACTORS

3.1 Multiscale modelling frameworks for gas phase catalytic polymerization

According to the definition provided by Ray (1986, 1991),[10,13] the multiscale modelling framework can be divided into three different length and time scales based on the characteristics and phenomena occurring in the polymerization systems as follows:

(1) Microscale (kinetic modelling): defined at the molecular level at which the polymerization kinetics take place at the active sites on the order of Angstroms (10^{-10} to 10^{-8} m).

(2) Mesoscale (mass and heat transport, and thermodynamic modelling): starting from catalyst particles to polymer particles with characteristic diameters on the order of 10^{-6} to 10^{-3} m. This scale involves the interphase phenomena including the sorption (i.e. gaseous species transfer from the continuous phase through the boundary around the particle), and the intraphase phenomena (i.e. transport or diffusion from the particle surface through the polymer particle), until the reaching of thermodynamic equilibria. This scale also concerns heat transfer through the particle. Besides, catalyst fragmentation, polymer particle morphology development, and interaction between particles (causing aggregation or breakage) occur.

(3) Macroscale (reactor modelling and control): defined at the reactor level and taking into account the hydrodynamics (macromixing), residence time distribution (RTD), heat and mass transfer in the reactor, and overall material and energy balances, as well as process optimization and control, with characteristic volumes on the order of cubic meters.

The detailed summary of multiscale modelling for gas phase olefin polymerization is presented in Table 3. The characteristic length and time scales here should be taken more as a rough guideline than as strict limits for reasons we will discuss below. The relationships between the three modelling scales in the case of polyolefin production in MZCR is presented in Figure 8.

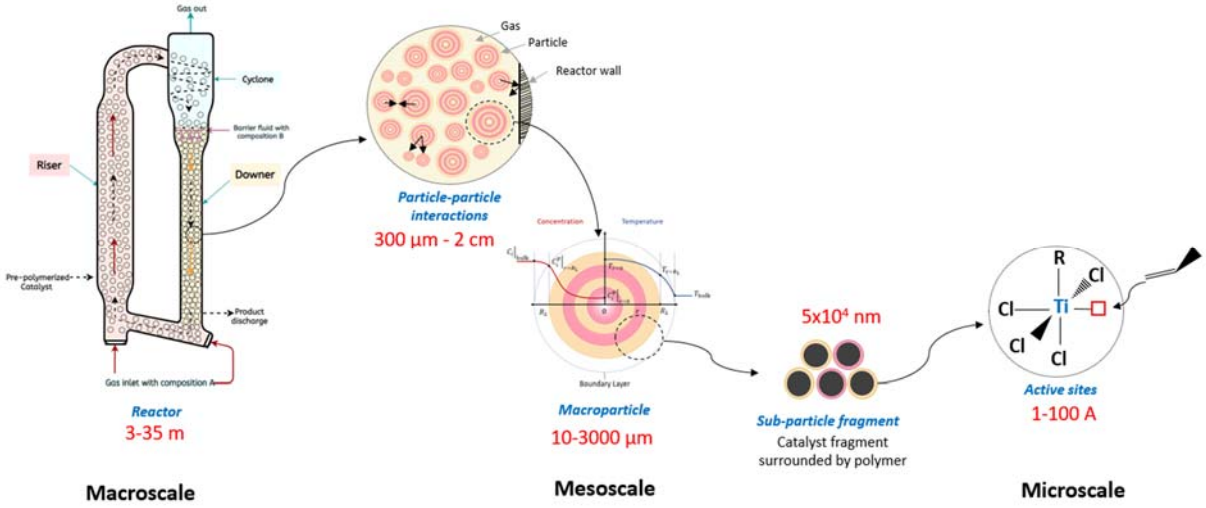

FIGURE 8 Schematic representation of a multiscale framework with three different length and time scales in a multi-volume polymerization reactor according to Ray[10,13]

It should be pointed out that boundaries of these three modelling scales are not clearly defined, as these scales are often overlapped due to the complex nature of the gas phase polyolefin reactors and the strong interaction between polymerization kinetics, thermodynamics, heat and mass transfer phenomena, and hydrodynamics.[9] However, the connection between the different scales might represent a challenge at the conceptual and computational levels. As suggested in Figure 8, one could easily define more than three length (and time) scales for this type of process.

Soares and McKenna[40] proposed up to 7 potential levels of complexity for the study of olefin polymerization reactors. Zhu et al.[41] developed a multiscale model to describe the particle behavior in propylene polymerization in an FBR. According to their work, the multiscale phenomenon may occur at 5 scales; namely, molecular scale (reaction kinetics), microscale (catalyst particle), mesoscale (polymer particle), macroscale (polymerization reactor), and plant scale (full process plant), while their multiscale modeling is defined by the same 3 scales defined above. Touloupidis[11] employed 3 modelling length scales for both slurry gas phase polymerization reactors, and proposed a procedure for the estimation of kinetic rate constants. In their work, the microscale includes kinetic modelling, the mesoscale includes thermodynamic modelling (without single particle modeling), and the macroscale includes reactor modelling. Dompazis et al.[15,18] developed a multiscale model to describe morphological (i.e. PSD) and molecular polymer properties (i.e. average molecular weights and MWD) for gas phase ethylene–propylene copolymerization over a multisite ZN catalyst, in an FBR, and identified 4 different length scales: a kinetic molecular scale, a microscale for

particle-level events, a mesoscale for particle interactions, and a macroscale for reactor level phenomena.

For gas phase catalytic olefin polymerization multizone reactors, the 3 level approach proposed by Ray[10] can be applied, as fewer levels of detail are not sufficient to cover the entire process. This said, aside from the papers mentioned above, most of the researchers focused on the micro- or macro- scales, and only few groups developed a complete multiscale model for multizone gas phase polymerization reactors. We will return to this point in Section 4.

Santos et al.[16,17] were the first to employ a fairly complete multiscale framework (including a kinetic model, a single particle model, and a reactor model) to the MZCR for propylene homo- and copolymerization. Later, Tian Z. et al.[42] applied the multiscale approach to predict the polymer PSD of propylene polymerization in the HSBRs. However, in these models, thermodynamic modelling was quite simple, as Henry's law was used to predict the concentrations of monomer and comonomer at the active sites. As we will see in section 3.3, thermodynamic models can significantly affect the monomer and comonomer concentrations, and thus the polymerization rate, especially under high pressure.

A summary of the implemented partial and full multiscale modelling framework for the gas phase multizone catalytic polymerization reactors including the MZCR, the FBR with internal circulation, and the HSBR is shown in Table 4. Before discussing specific reactor models, we will provide an emphasis of the issues that need to be addressed at each modelling scale, with a focus on gas phase propylene polymerization. Obviously, this analysis can be extended to slurry or mixed phase reactors, as well as to ethylene homo- and copolymerization with specific adjustments required at different points.

3.2 Microscale: Molecular level

Many researchers, far too numerous to enumerate in the current paper (readers are referred to references [17,51–57] for an overview of some of these works), have studied the homo- and copolymerization kinetics of polypropylene produced with solid catalysts including high-activity supported $TiCl_4/MgCl_2$ Ziegler–Natta, unsupported $TiCl_3$, and recently commercialized Metallocene systems. In general, the ZN catalysts are multi-sites, which leads to the production of polyolefins with broad MWD. Typically, these catalysts are said to contain between 3 and 6 sites;[50,57–59] where each site has its own set of kinetic parameters, leading to different reaction rates and properties (e.g. chain length and comonomer fraction in polymer).[60,61]

TABLE 3 Summary of the multiscale modelling for gas phase olefin polymerization.[9–12]

	Microscale	Mesoscale	Macroscale
Time scales	$< 10^0$ seconds	$\leq 10^2$ seconds	$> 10^2$ seconds
Length scales	Angstrom	Micrometers	Meters
Level	Molecular	Single particle and its boundary layer	Reactor
Model	Kinetics Examples: - Kinetic Monte Carlo simulation - Global kinetics	- Mass and heat transfer: e.g. Single Particle Models (SPM) such as PFM/ RPPFM, and MGM - SPM coupled with a CFD model - Diffusion models - Thermodynamic models (e.g. Henry's law, Sanchez-Lacombe EoS, SAFT/PC-SAFT) - Particle morphology - Breakage and aggregation kernels	Overall momentum, mass, and energy balances, population balance model: (adapted to the reactor geometry, CSTR, PFR, etc.) Example: - Compartmentalized models - Hydrodynamic models
Model outputs	Molecular structure properties (i.e., $\overline{M}_n$, $\overline{M}_w$, PI, MWD, CCD), reaction rate in bulk	- Concentration and temperature gradients inside polymer particle - Diffusion rate of gaseous species in the amorphous phase - Solubility of monomer(s) and other species into the amorphous polymer at equilibrium - Polymerization rate and particle growth rate - Evolution of the PSD	- Evolution of temperature and concentrations (of monomer, other gases, particles of different sizes) in time and in space - Reactor performances (productivity, conversion, etc.) - Product qualities (i.e., $\overline{M}_n$, $\overline{M}_w$, PI, MWD, CCD, PSD, etc.) in time and in space - End-use properties (density, melt index)

TABLE 4 Summary of the implemented (partial and full) multiscale framework for gas phase multizone olefin polymerization reactors.

Reference	Systems (Monomer/ Comonomer)	Microscale		Mesoscale		Macroscale		
		Reactions	Catalyst/ No of site types	Thermodynamic model	SPM	Reactor type	No of zones	Zone/ Flow regime/ Model
Fernandes et al.[43,44]	PE (LLDPE) (Ethylene/1-butene)	- Site activation - Chain initiation - Propagation - Chain transfer to monomer, comonomer, hydrogen	ZN / 1 site	$C_i^{amp}=C_i^{bulk}$	-	MZCR	2	1. Riser/Fast fluidization regime/PFR 2. Downer/Moving packed bed regime/PFR
Adli et al.[45]	PE (LLDPE) (Ethylene/1-butene)	- Site activation - Chain initiation - Propagation - Chain transfer to monomer, comonomer, hydrogen	ZN / 1 site	$C_i^{pol}=C_i^{bulk}$	-	MZCR	2	1. Riser/Fast fluidization regime/PFR 2. Downer/Moving packed bed regime/PFR

Reference	Systems (Monomer/ Comonomer)	Microscale		Mesoscale		Macroscale		
		Reactions	Catalyst/ No of site types	Thermodynamic model	SPM	Reactor type	No of zones	Zone/ Flow regime/ Model
Ghasem et al.[46,47]	PE (LLDPE) (Ethylene/1-butene)	- Site activation - Chain initiation - Propagation - Chain transfer to monomer, comonomer, hydrogen	ZN / 1 site	$C_i^{pol}=C_i^{bulk}$	-	MZCR	2	1. Riser/Fast fluidization regime/PFR 2. Downer/Moving packed bed regime/PFR
Santos et al.[16,17]	PP (HPP and RCP) (Propylene/ethylene)	- Chain initiation - Propagation - Chain transfer to hydrogen	ZN / 1 site	Henry's law	Multigrain model (MGM)	MZCR	2	1. Riser/Fast fluidization regime/PFR 2. Downer/Moving packed bed regime/PFR
Meier et al.[48]	PP-HPP (Propylene)	- Chain Initiation - Propagation - Catalyst site deactivation	Metallocene	- Flory-Huggins Equation - Peng-Robinson Equation	-	FBR-IC	3	1. Annulus zone/Moving packed bed regime/PFR 2. Draft tube zone/Fast fluidization regime/PFR 3. Cone zone/Perfectly mixed phase/CSTR

Reference	Systems (Monomer/ Comonomer)	Microscale		Mesoscale		Macroscale		
		Reactions	Catalyst/ No of site types	Thermodynamic model	SPM	Reactor type	No of zones	Zone/ Flow regime/ Model
Zacca et al.[49]	PP-HPP and ICP (Propylene/ethylene)	- Catalyst Site activation - Chain Initiation - Propagation - Chain transfer to hydrogen - Catalyst site deactivation - Site transformation	ZN / 2 sites	Benedict Webb-Rubin equation of state (BWR EoS)	-	HSBR/VSBR/ FBR	4	CSTR/Perfectly mixed phase/4 CSTRs in series
Khare et al.[50]	PP-HPP and ICP (Propylene/ethylene)	- Catalyst Site activation - Chain Initiation - Propagation - Chain transfer to hydrogen - Catalyst site deactivation	ZN / 4 sites	PC-SAFT EoS (binary system)	-	HSBR	4	CSTR/Perfectly mixed phase/4 CSTRs in series
Tian et al.[42]	PP-HPP	- Catalyst Site activation - Propagation - Catalyst site deactivation	ZN / 1 site	Henry's law	Polymer multilayer model (PMLM)	HSBR	4	CSTR/Perfectly mixed phase/4 CSTRs in series

Good overviews of the possible kinetic schemes in olefin polymerizations in slurry and gas phase ZN catalysts are given by Touloupidis[11] and Thakur et al.[61] The elimination of some elementary steps is typically made to simplify the development of the kinetic model, while retaining the ability to accurately estimate the overall polymerization rate and polymer average molecular weight.

In this review, we will pay particular attention to propylene homopolymerization and propylene-ethylene copolymerization kinetics with supported Ziegler−Natta catalysts. Table 5 shows the general kinetic mechanisms for propylene-ethylene copolymerization over a multi-site Ziegler-Natta catalyst ("*k*" refers to the site number). The reactions include catalyst activation (mostly with cocatalyst, but can be spontaneous), chain initiation, propagation, chain transfer (mostly to hydrogen), spontaneous chain termination, formation and reactivation of dormant site and thermal site deactivation. The homopolymerization kinetics can obviously be obtained by eliminating all reactions involving ethylene. It should be noted that the most common chain transfer reaction is by hydrogen, with only little possible chain transfer to monomer, comonomer, solvent, cocatalyst, or spontaneous chain transfer.

Regarding the hydrogen response, it is well-known that hydrogen not only acts as a CTA in polyolefin polymerization, but it also influences the polymerization rate, depending on the monomer. Indeed, it was found by several researchers[62–64] that transfer to hydrogen may lead to a decrease in the reaction rate in ethylene polymerization. In propylene polymerization, it leads to an increase in the reaction rate at low hydrogen concentrations, but adding hydrogen at moderate to high concentrations may decrease the propylene polymerization rate,[65–67] These findings are explained by the so-called "dormant site theory".[65–67]

In the dormant site theory, propylene can either be inserted into a growing polymer chain by primary 1,2 insertion (Figure 9a) or a secondary 2,1 insertion (or regioirregular insertion) (Figure 9b). When inserting with regioirregular 2,1 insertion, the methyl group of propylene can block the activated Ti atom on the catalyst, creating a temporarily dormant or sleeping site; the active site is not deactivated but sterically blocked. When hydrogen is added, it is suggested that it is small enough to pass through the methyl group and decouple the growing polymer chain by reacting with the Ti-polymer chains (Figure 9c). The vacant active site is then converted to a transition metal hydride Ti─H bond that can be reactivated by propylene or ethylene in the re-initiation and propagation steps. At low to moderate hydrogen levels, this

leads to an increase in the reaction rate in propylene polymerization, compared to reactions done in the absence of hydrogen.

(a)

(b)

(c)

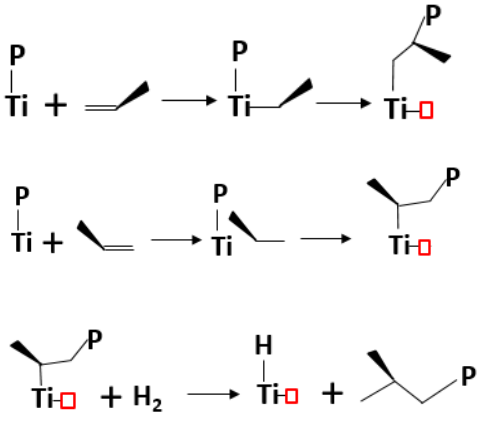

FIGURE 9 Formation and reactivation of dormant sites: (a) Primary 1,2–Insertion of propylene, (b) Secondary 2,1–Insertion of propylene to create a dormant site, (c) Chain transfer to Hydrogen after 2,1–Insertion to free up a dormant site, adapted from Ali et al. [65] and Putten [68]

Several modelling approaches can be adopted to calculate the reaction rate based on the reaction scheme shown in Table 5, such as population balance modelling of the chain length (on which the method of moments can be applied) or the kinetic Monte Carlo method. The method of moments is the most commonly used due to its simplicity and less numerical effort.[6,11,69] Excellent reviews of the modelling methods used for the calculation of the molecular properties (e.g. the number and weight-average molecular weights and the polydispersity index) can be found in references.[69,70] Assuming a single site catalyst and using the method of moments, the net reaction rates of the molecular species and the polymer chains in the supported ZN olefin polymerization are given in Table 6.

The chain length (or molecular weight) averages can be estimated from the moments of the chain length distribution (i.e. living and dead moments) as follows:

Number-average molecular weight of polymer ($\overline{Mn}$) is defined as:

$$\overline{Mn} = W\left(\frac{\mu_1+\lambda_1}{\mu_0+\lambda_2}\right) \quad (1)$$

TABLE 5 Generalized kinetic schemes of gas phase copolymerization of propylene (1) and ethylene (2) over a Ziegler-Natta catalyst for multi-site type "*k*" catalyst.

Type of reaction	Kinetic mechanism	Kinetic rate coefficients	Reaction description	References
Site activation by cocatalyst	$S_{\mathrm{p}}^{k} + Co \xrightarrow{k_{\mathrm{a}}^{k}} P_{0}^{k}$	k_{a}^{k}	The potential catalyst active site (S_{p}^{k}) is activated by cocatalyst to create a vacant active site (P_{0}^{k})	[49,51,53,55–57]
Chain initiation	$P_{0}^{k} + C_{1} \xrightarrow{k_{\mathrm{i},1}^{k}} P_{1,1}^{k}$	$k_{\mathrm{i},1}^{k} = k_{0\mathrm{i},1}^{k} \mathrm{e}^{\frac{-Ea_{\mathrm{i},1}^{k}}{RT}}$	The vacant active site (P_{0}^{k}) reacts with monomer (C_1) and comonomer (C_2) to produce living polymer chains with chain length 1, ($P_{1,1}^{k}$ and $P_{1,2}^{k}$)	[49,51,53,55–57]
	$P_{0}^{k} + C_{2} \xrightarrow{k_{\mathrm{i},2}^{k}} P_{1,2}^{k}$	$k_{\mathrm{i},2}^{k} = k_{0\mathrm{i},2}^{k} \mathrm{e}^{\frac{-Ea_{\mathrm{i},2}^{k}}{RT}}$		
Re-initiation	$P_{0\mathrm{H}}^{k} + C_{1} \xrightarrow{k_{\mathrm{iH},1}^{k}} P_{1,1}^{k}$	$k_{\mathrm{iH},1}^{k} = k_{0\mathrm{iH},1}^{k} \mathrm{e}^{\frac{-Ea_{\mathrm{iH},1}^{k}}{RT}}$	The vacant active site with Ti─H bond ($P_{0\mathrm{H}}^{k}$) react with monomer (C_1) and comonomer (C_2) to form living polymer chains with chain length 1, ($P_{1,1}^{k}$ and $P_{1,2}^{k}$)	[65–68,71]
	$P_{0\mathrm{H}}^{k} + C_{2} \xrightarrow{k_{\mathrm{iH},2}^{k}} P_{1,2}^{k}$	$k_{\mathrm{iH},2}^{k} = k_{0\mathrm{iH}2}^{k} \mathrm{e}^{\frac{-Ea_{\mathrm{iH},2}^{k}}{RT}}$		
Propagation	$P_{n,1}^{k} + C_{1} \xrightarrow{k_{\mathrm{p}11}^{k}} P_{n+1,1}^{k}$	$k_{\mathrm{p}11}^{k} = k_{0\mathrm{p},11}^{k} \mathrm{e}^{\frac{-Ea_{\mathrm{p}11}^{k}}{RT}}$	The polymer chain grows during the propagation step, a new monomer (C_1) or comonomer (C_2) is inserted between the catalyst site and the living polymer chain with chain length n ($P_{n,1}^{k}$ or $P_{n,2}^{k}$) to increase	[49,51,53–57]
	$P_{n,2}^{k} + C_{1} \xrightarrow{k_{\mathrm{p}21}^{k}} P_{n+1,1}^{k}$	$k_{\mathrm{p}21}^{k} = k_{0\mathrm{p},21}^{k} \mathrm{e}^{\frac{-Ea_{\mathrm{p}21}^{k}}{RT}}$		
	$P_{n,1}^{k} + C_{2} \xrightarrow{k_{\mathrm{p}12}^{k}} P_{n+1,2}^{k}$	$k_{\mathrm{p}12}^{k} = k_{0\mathrm{p},12}^{k} \mathrm{e}^{\frac{-Ea_{\mathrm{p}12}^{k}}{RT}}$		
	$P_{n,2}^{k} + C_{2} \xrightarrow{k_{\mathrm{p}22}^{k}} P_{n+1,2}^{k}$			

Type of reaction	Kinetic mechanism	Kinetic rate coefficients	Reaction description	References
		$k_{\mathrm{p}22}^{k} = k_{0\mathrm{p},22}^{k}\mathrm{e}^{\frac{-Ea_{\mathrm{p}22}^{k}}{RT}}$	the polymer chain length by one unit ($P_{n+1,1}^{k}$ or $P_{n+1,2}^{k}$)	
Chain transfer to hydrogen	$P_{n,1}^{k} + \mathrm{H}_2 \xrightarrow{k_{\mathrm{tH},1}^{k}} P_{0\mathrm{H}}^{k} + D_n^{k}$ $P_{n,2}^{k} + \mathrm{H}_2 \xrightarrow{k_{\mathrm{tH},2}^{k}} P_{0\mathrm{H}}^{k} + D_n^{k}$	$k_{\mathrm{tH},1}^{k} = k_{0\mathrm{tH},1}^{k}\mathrm{e}^{\frac{-Ea_{\mathrm{tH},1}^{k}}{RT}}$ $k_{\mathrm{tH},2}^{k} = k_{0\mathrm{tH},2}^{k}\mathrm{e}^{\frac{-Ea_{\mathrm{tH},2}^{k}}{RT}}$	The living polymer chains ($P_{n,1}^{k}$ and $P_{n,2}^{k}$) are terminated by transfer to hydrogen (H_2) to produce a dead polymer chain (D_n^{k}), and a vacant active site with Ti─H bond ($P_{0\mathrm{H}}^{k}$) which is able to react further in the re-initiation step.	[49,51,53,55–57]
Spontaneous chain termination	$P_{n,1}^{k} \xrightarrow{k_{\mathrm{d},1}^{k}} D_n^{k}$ $P_{n,2}^{k} \xrightarrow{k_{\mathrm{d},2}^{k}} D_n^{k}$	$k_{\mathrm{d},1}^{k}$ $k_{\mathrm{d},2}^{k}$	The active site can be deactivated spontaneously to form a dead polymer chain	[49,51,53–57]
Formation of dormant sites	$P_{n,1}^{k} + C_1 \xrightarrow{k_{\mathrm{dor},1}^{k}} S_n^{k}$ $P_{n,2}^{k} + C_1 \xrightarrow{k_{\mathrm{dor},2}^{k}} S_n^{k}$	$k_{\mathrm{dor},1}^{k}$ $k_{\mathrm{dor},2}^{k}$	Secondary 2,1 insertion of propylene into the growing polymer chain creates a dormant chain (S_n^{k})	[65–68,71]
Reactivation of dormant site by hydrogen	$S_n^{k} + \mathrm{H}_2 \xrightarrow{k_{\mathrm{rH}}^{k}} P_{0\mathrm{H}}^{k} + D_n^{k}$	k_{rH}^{k}	The inactive dormant chain is reactivated by H_2 to create a vacant active site with Ti─H bond and a dead polymer chain	[65–68,71]

Type of reaction	Kinetic mechanism	Kinetic rate coefficients	Reaction description	References
Reactivation of dormant site by spontaneous reaction	$S_n^k \xrightarrow{k_r^k} P_{n+1,1}^k$	k_r^k	The reactivation of the dormant site may occur spontaneously to form a growing polymer with chain length 1	[65–68,71]
Site deactivations by Thermal	$S_p^k \xrightarrow{k_{d,T}^k} S_{p,d}^k$	$k_{d,T}^k = k_{0d,T}^k e^{\frac{-Ea_{d,T}^k}{RT}}$	The potential active deactivates due to overheating at high temperature to form a dead site	[71]

Weight-average molecular weight of polymer ($\overline{Mw}$) is given by:

$$\overline{Mw} = W\left(\frac{\mu_2+\lambda_2}{\mu_1+\lambda_1}\right) \quad (2)$$

Polydispersity index of the chain length distribution (PI) is given by:

$$PI = \frac{\overline{Mw}}{\overline{Mn}} \quad (3)$$

Where W is the average molecular weight of monomer species inserted into the chain:

$$W = \frac{\sum_{j=1}^{2} Mw_j C_j^{\mathrm{P}}}{\sum_{j=1}^{2} C_j^{\mathrm{P}}} \quad (4)$$

Where Mw_j is the molecular weight of the monomer (or comonomer) j and C_j^{P} is the concentration of monomer at the active sites.

The kinetic coefficients in Table 5 follow Arrhenius equation, which implies the temperature dependence of the reaction rates:

$$k_j^k = k_{0,j}^k e^{\frac{-Ea_j^k}{RT}} \quad (5)$$

Where k_0 is the pre-exponential factor of the kinetic coefficient ($m^3\ mol^{-1}s^{-1}$ for 2nd order rate constant; or s^{-1} for 1st order rate constant), Ea is the activation energy for the reaction (J mol^{-1}), R is the universal gas constant (J $mol^{-1}K^{-1}$) and T is the reaction temperature (K). Superscript "k" is the number of the employed catalyst active sites, and subscript "j" is the notation for the elementary reactions.

Note that in catalytic polymerization, the propagation rate coefficients are specific for the studied polymerization system (i.e. catalyst system, and monomer) and they may vary with time due to catalyst deactivation. This makes catalytic polymerization more difficult to model than other mechanisms, like free radical or ionic polymerization. The estimation of these parameters (k_0 and Ea) and/or reactivity ratios values (k_{11}/k_{12} and k_{22}/k_{21}) can be done by fitting with experimental data related to the polymer production rate, the polymer microstructure properties (e.g. MWDs, CCDs, etc.) as well as the end-use properties (i.e.

polymer density and melt index). Several procedures for the estimation of the kinetic parameters are discussed elsewhere.[11,50,57,61,66,72,73]

Finally, it is important to state that the set of equations (Equations 6-21) in Table 6 is highly coupled with the mesoscale model (thermodynamics and transport) and with the macroscale model (concentrations and temperature in space in the reactor).[11] Indeed, the accuracy of the kinetic model depends on how accurately one can estimate the concentrations of the active species and temperature at the catalyst sites, appearing in the reaction rate equations. The challenges associated with current state of the kinetic modeling for the propylene (co)polymerization will be discussed in detail, later in section 4.1.

TABLE 6 Reaction rates of the molecular species and the moment chains in supported ZN olefin polymerization with a single site catalyst, derived by the method of moments of chain lengths[a].

Species	**Reaction rate**	**No. of Equation**
Potential active site produced	$R_{Sp} = -k_a[S_p] - k_{d,T}[S_p]$	(6)
Site deactivation	$R_{Sp,d} = k_{d,T}[S_p]$	(7)
Vacant activated sites	$R_{P0} = k_a[S_p] - (k_{i,1}C_1^P + k_{i,2}C_2^P)[P_0]$	(8)
Vacant activated sites with a Ti—H bond	$R_{P0H} = -(k_{iH,1}C_1^P + k_{iH,2}C_2^P)[P_{0H}] + k_{rH}(C_{H_2}^P)^{\frac{1}{2}}\eta_0 + (k_{tH,1}\phi_1 + k_{tH,2}\phi_2)\lambda_0(C_{H_2}^P)^{\frac{1}{2}}$	(9)
Monomers	$R_1 = \{k_{i,1}[P_0] + k_{iH,1}[P_{0H}] + (k_{p_{11}}\phi_1 + k_{p_{21}}\phi_2)\lambda_0\}C_1^P$	(10)
	$R_2 = \{k_{i,2}[P_0] + k_{iH,2}[P_{0H}] + (k_{p_{12}}\phi_1 + k_{p_{22}}\phi_2)\lambda_0\}C_2^P$	(11)
Hydrogen	$R_{H_2} = (k_{tH,1}\phi_1 + k_{tH,2}\phi_2)\lambda_0(C_{H_2}^P)^{\frac{1}{2}} - k_{rH}(C_{H_2}^P)^{\frac{1}{2}}\eta_0$	(12)

Living chains 0th moment	$R_{\lambda 0} = \left(k_{\mathrm{i},1} C_1^{\mathrm{P}} + k_{\mathrm{i},2} C_2^{\mathrm{P}}\right)[P_0] + \left(k_{\mathrm{iH},1} C_1^{\mathrm{P}} + k_{\mathrm{iH},2} C_2^{\mathrm{P}}\right)[P_{0\mathrm{H}}] + k_{\mathrm{r}}\eta_0 - \lambda_0 \left\{\left(k_{\mathrm{dor},1}\phi_1 + k_{\mathrm{dor},2}\phi_2\right) C_1^{\mathrm{P}} + \left(k_{\mathrm{tH},1}\phi_1 + k_{\mathrm{tH},2}\phi_2\right)(C_{\mathrm{H}_2}^{\mathrm{P}})^{\frac{1}{2}} + k_{\mathrm{d}}\right\}$	(13)
1st moment	$R_{\lambda 1} = (k_{\mathrm{i}1} C_1^{\mathrm{P}} + k_{\mathrm{i}2} C_2^{\mathrm{P}})[P_0] + (k_{\mathrm{iH}1} C_1^{\mathrm{P}} + k_{\mathrm{iH}2} C_2^{\mathrm{P}})[P_{0\mathrm{H}}] + k_{\mathrm{r}}\eta_1 + \lambda_0\{\left(k_{\mathrm{p}_{11}}\phi_1 + k_{\mathrm{p}_{21}}\phi_2\right) C_1^{\mathrm{P}} + \left(k_{\mathrm{p}_{12}}\phi_1 + k_{\mathrm{p}_{22}}\phi_2\right) C_2^{\mathrm{P}}\} - \lambda_1 \left\{\left(k_{\mathrm{dor},1}\phi_1 + k_{\mathrm{dor},2}\phi_2\right) C_1^{\mathrm{P}} + \left(k_{\mathrm{tH},1}\phi_1 + k_{\mathrm{tH},2}\phi_2\right)(C_{\mathrm{H}_2}^{\mathrm{P}})^{\frac{1}{2}} + k_{\mathrm{d}}\right\}$	(14)
2nd moment	$R_{\lambda 2} = \left(k_{\mathrm{i},1} C_1^{\mathrm{P}} + k_{\mathrm{i},2} C_2^{\mathrm{P}}\right)[P_0] + \left(k_{\mathrm{iH},1} C_1^{\mathrm{P}} + k_{\mathrm{iH},2} C_2^{\mathrm{P}}\right)[P_{0\mathrm{H}}] + k_{\mathrm{r}}\eta_2 + (\lambda_0 + 2\lambda_1)\{\left(k_{\mathrm{p}_{11}}\phi_1 + k_{\mathrm{p}_{21}}\phi_2\right) C_1^{\mathrm{P}} + \left(k_{\mathrm{p}_{12}}\phi_1 + k_{\mathrm{p}_{22}}\phi_2\right) C_2^{\mathrm{P}}\} - \lambda_2 \left\{\left(k_{\mathrm{dor},1}\phi_1 + k_{\mathrm{dor},2}\phi_2\right) C_1^{\mathrm{P}} + \left(k_{\mathrm{tH},1}\phi_1 + k_{\mathrm{tH},2}\phi_2\right)(C_{\mathrm{H}_2}^{\mathrm{P}})^{\frac{1}{2}} + k_{\mathrm{d}}\right\}$	(15)
Dead chains		
0th moment	$R_{\mu_0} = \lambda_0 \left(k_{\mathrm{d}} + k_{\mathrm{tH}}(C_{\mathrm{H}_2}^{\mathrm{P}})^{\frac{1}{2}}\right) + \eta_0 \left(k_{\mathrm{rH}}(C_{\mathrm{H}_2}^{\mathrm{P}})^{\frac{1}{2}} + k_{\mathrm{r}}\right)$	(16)
1st moment	$R_{\mu_1} = \lambda_1 \left(k_{\mathrm{d}} + k_{\mathrm{tH}}(C_{\mathrm{H}_2}^{\mathrm{P}})^{\frac{1}{2}}\right) + \eta_1 k_{\mathrm{rH}}(C_{\mathrm{H}_2}^{\mathrm{P}})^{\frac{1}{2}}$	(17)
2nd moment	$R_{\mu_2} = \lambda_2 \left(k_{\mathrm{d}} + k_{\mathrm{tH}}(C_{\mathrm{H}_2}^{\mathrm{P}})^{\frac{1}{2}}\right) + \eta_2 k_{\mathrm{rH}}(C_{\mathrm{H}_2}^{\mathrm{P}})^{\frac{1}{2}}$	(18)
Dormant chains		
0th moment	$R_{\eta_0} = \lambda_0 C_1^{\mathrm{P}}\left(k_{\mathrm{dor},1}\phi_1 + k_{\mathrm{dor},2}\phi_2\right) - \eta_0 \left(k_{\mathrm{rH}}(C_{\mathrm{H}_2}^{\mathrm{P}})^{\frac{1}{2}} + k_{\mathrm{r}}\right)$	(19)
1st moment	$R_{\eta_1} = \lambda_1 C_1^{\mathrm{P}}\left(k_{\mathrm{dor},1}\phi_1 + k_{\mathrm{dor},2}\phi_2\right) - \eta_1 \left(k_{\mathrm{rH}}(C_{\mathrm{H}_2}^{\mathrm{P}})^{\frac{1}{2}} + k_{\mathrm{r}}\right)$	(20)
2nd moment	$R_{\eta_2} = \lambda_2 C_1^{\mathrm{P}}\left(k_{\mathrm{dor},1}\phi_1 + k_{\mathrm{dor},2}\phi_2\right) - \eta_2 \left(k_{\mathrm{rH}}(C_{\mathrm{H}_2}^{\mathrm{P}})^{\frac{1}{2}} + k_{\mathrm{r}}\right)$	(21)

[a] $\phi_1 = \frac{k_{p_{21}} C_1^P}{k_{p_{21}} C_1^P + k_{p_{12}} C_2^P}$ and $\phi_2 = 1 - \phi_1 = \frac{k_{p_{12}} C_2^P}{k_{p_{21}} C_1^P + k_{p_{12}} C_2^P}$

3.3 Mesoscale: Single particle level and its boundary layer

Discussions about modeling particle-particle agglomeration, particle break-up and interactions between the particles and internal fixtures in the reactor can be found in other review.[19] In this review, the discussion will consider events at the mesoscale to include the polymer particle and its boundary layer only.

Figure 10 shows a schematic representation of the interphase phenomena, including heat and mass transfer across the boundary layer surrounding the growing polymer particle.[74,75] In gas phase ZN olefin polymerizations, the gaseous monomer and comonomer(s) are transported from the continuous gas phase of the reactor to the external particle surface through the boundary layer surrounding the polymer particle. Consequently, the gas species are transferred through the polymer particle pores and through the amorphous polymer phase surrounding the active sites. The heat, generated by the polymerization at the active sites, is transferred in the inverse direction.[74]

It is well-known that thermodynamic equilibrium and transport (i.e. heat and mass transfer) both play a significant role in the polymerization rate and polymer properties (i.e. molecular property and particle morphology).[11] Indeed, single particles models allow one to describe the diffusion of monomer(s) in the particle (so they do not assume equilibrium), but equilibrium values are required as boundary conditions for this model. Therefore, precise calculation of solubilities and diffusivities is very important in multicomponent mixtures. Despite the importance of this last point, Alves et al.[19] showed that virtually no complete modelling studies included thermodynamic models that included the complex co- and anti-solubility effects that are present in multicomponent mixtures dissolving in polyolefins. They also showed that ignoring these effects might lead to an under-prediction of the ethylene and ICA concentrations in amorphous PE, and consequently to the underestimation of the production rate.[76]

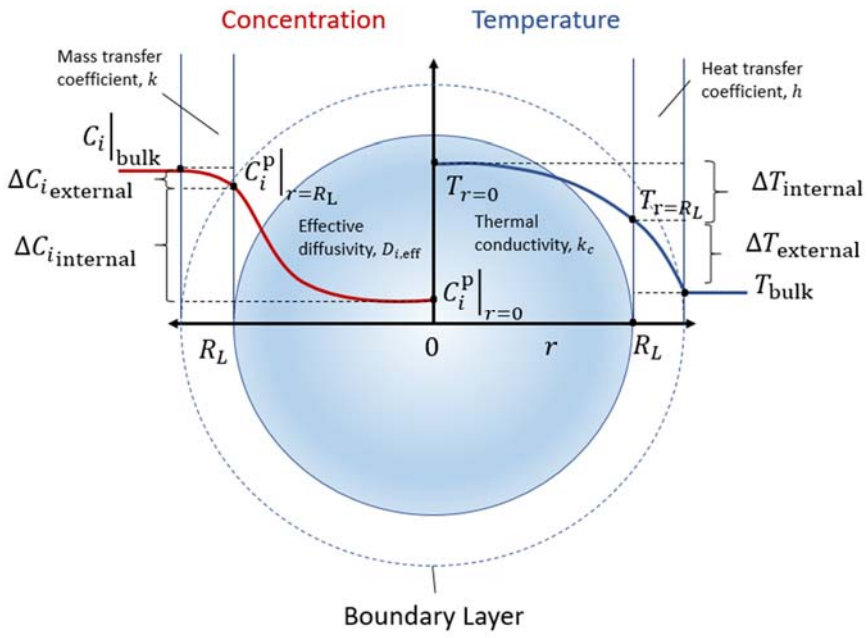

FIGURE 10 Schematic representation of the interphase phenomena (concentration and temperature gradients) of a single particle made in gas phase catalytic olefin polymerization at the mesoscale, adapted from Soares and McKenna[74] and Floyd et al.[75]

In the following subsections, an example of single particle model is presented. Then, we discuss the methods used to predict equilibrium concentrations in the amorphous polymer phase and we apply them to propylene-ethylene copolymerization. The models used to calculate the diffusion coefficients of monomer into the polymer particle (taking into account codiffusivity effects) are not presented, but recent reviews are provided. Similarly, for a review on the particle morphology models, the reader is referred to the work of Alizadeh and Mckenna,[77] and will not be discussed here.

3.3.1 Single particle models

Several single particle models have been proposed to describe the particle growth phenomenon.[75,78–83] Among them, the multigrain model (MGM) and the polymeric flow model (PFM) are the most commonly used models to estimate the concentration and temperature profiles inside the particle and predict its growth rate during the olefin polymerization.[22] A good overview and comparison of the several single particle models can be found in reference .[61] The development and solution strategies of the SPMs have been extensively discussed in

the literatures: see for instance Floyd et al.,[75] Hutchinson et al.,[84] Debling and Ray,[85] McKenna and Soares,[86] Kanellopoulos et al.,[83] Alizadeh and Mckenna,[77] McKenna and Ahsan,[12] and Ben Mrad et al.[87]

If one makes the assumption that mass transfer is controlled by diffusion, then the importance of mass transfer resistance to monomer transport from the bulk phase to the active sites will be determined by the competition between the reaction and the diffusion rates. Increasing the polymerization rate can lead to the reduction of monomer availability in the centre of the particles. Furthermore, anything that increases the characteristic time for diffusion will have a similar effect. As diffusion through the pores is much faster than diffusion through the polymer that covers the active sites, the characteristic thickness of the polymer layer (i.e. the polymer particle morphology, or shape) is the determinant factor here. It is well-known that the morphology of the real catalysts/particles and their physical properties (i.e. particle porosity, pore size and size distribution) will change depending on the process and operating condition.[12,74,77] This is one of the major challenges for developing particle level models.

Different models have been proposed, including the multigrain model,[74] where the particle (the polymer macrograin) is assumed be a collection of concentric layers of polymer micrograins. As discussed by McKenna et al.,[88] this is now generally taken to be unrealistic and mathematically cumbersome. For this reason, most authors use some version of what is known as the polymeric flow model (PFM), (also referred to as the polymer multilayer model PMLM, or random pore polymeric flow model RPPFM).[83] In the PFM, the growing polymer particle is treated as a pseudo-homogeneous medium composed of a mixture of polymer space and pore space, in which the active sites are dispersed uniformly. The PFM has the advantage of being relatively simpler compared to other SPMs, and if one knows the particle porosity (a very big "if"), it is possible to propose a realistic value for the diffusivity through the particle. However, as mentioned above, this requires *a priori* knowledge of the particle morphology (as a function of time and instantaneous reactor conditions), which is not possible. This model gives us good approximation of particle level phenomena, but remains a weak link in the modelling hierarchy.

General mass balances around a polymer particle in gas-phase systems (Figure 10), while neglecting the external mass transfer resistance across the particle boundary layer and assuming the fragmentation step of the polymer particle to be complete, can be written as follows:

$$\frac{\partial C_{i,\text{eff}}}{\partial t} = D_{i,\text{eff}} \frac{1}{r^2}\frac{\partial}{\partial r}\left(r^2 \frac{\partial C_{i,\text{eff}}}{\partial r}\right) - R_i \tag{22}$$

With the boundary conditions (for all *t*):

$$\text{At } r = 0$$
$$\frac{\partial C_{i,\text{eff}}}{\partial r}(r = 0, t) = 0 \tag{23}$$

$$\text{At } r = R_\text{L}$$
$$C_{i,\text{eff}}(r = R_\text{L}, t) = C_{i,\text{eff}}^{\text{eq}} \tag{24}$$

And the initial condition ($t = 0$):

$$C_{i,\text{eff}}(r, t = 0) = 0 \tag{25}$$

Where $C_{i,\text{eff}}$ is the overall effective concentration of species i per volume of entire pseudo-homogenous, t is the polymerization time, r is the radial position in the particle of radius R_L, $D_{i,\text{eff}}$ is the overall effective diffusivity of species i in the macroparticle and R_i is the polymerization rate of species i.

According to Equation (22), three important quantities need to be well-estimated: the polymerization rate (R_i) (which is related to the concentration of reactive species *i* in the amorphous phase and temperature, and to the microscale kinetic model), the boundary condition which is determined by thermodynamic equilibrium (see section 3.3.2), and the effective diffusivity in the macrograin ($D_{i,\text{eff}}$, see section 3.3.3), related to multicomponent solubility and sorption thermodynamics.

The energy balances in a polymer particle can be written as follows:

$$\rho^\text{p} C_{p,\text{p}} \frac{\partial T}{\partial t} = k_\text{c} \frac{1}{r^2}\frac{\partial}{\partial r}\left(r^2 \frac{\partial T}{\partial r}\right) + \left(-\Delta H_\text{p}\right) R_i \tag{26}$$

With the boundary conditions (for all *t)*:

$$\text{At } r = 0$$
$$\frac{\partial T}{\partial r}(r = 0, t) = 0 \tag{27}$$

At $r = R_{\mathrm{L}}$

$$k_c \frac{\partial T}{\partial r}(r = R_{\mathrm{L}}, t) = h(T_{\mathrm{b}} - T) \tag{28}$$

Initial Condition (t = 0):

$$T(r, t = 0) = T_{\mathrm{b}} \tag{29}$$

Where T is the local particle temperature inside the particle, k_{c} the effective thermal conductivity of the particle, ρ^{p} the global density of the particle, $C_{p,\mathrm{p}}$ the global heat capacity of the particle and ΔH_{p} is the heat of polymerization.

The external convective heat transfer coefficient (h) can be calculated using correlations for Nusselt number (Nu). It is worth mentioning that the external heat transfer resistance across the particle boundary layer should not be neglected (unlike the external mass transfer resistance) since the temperature difference between the continuous phase and the particle can be large for certain gas phase polymerizations (e.g. over 10°C), especially at the beginning of the polymerization. Therefore, the boundary condition of the energy balance in Equation (28) at the particle surface ($r = R_{\mathrm{L}}$) must account for the external heat transfer resistance. Furthermore, as discussed by Soares and McKenna,[86] modelling the external heat transfer coefficient is not a straightforward task. Particle-particle interactions can mean that conductive heat transfer between large and small particles is important. Therefore, Nu-based correlations should also take into account the nature of the particle powder bed.

Equations (22) and (26) are coupled and must be solved together with the kinetic model to estimate the concentration and temperature gradients in the growing polymer particle.

3.3.2 Thermodynamic models

Precise estimation of the solubility of a sorbed monomer/comonomer(s) in amorphous polymer is essential in order to obtain the concentrations at the active sites and determine the polymerization rate, especially when the cosolvent and antisolvent effects are significant. Cosolvent (or cosolubility) effect is referred to the enhancement of the solubility of the lighter component in the amorphous polymer when a heavier component is presented in the gas phase composition (the heavier the alkene or alkane, the greater the effect), the antisolvent or

antisolubility effect is, on the other hand, the presence of the lighter species decreasing the solubility of the heavier one.

There are several thermodynamic models to describe phase equilibrium, ranging from the simple Henry's law, to more advanced activity coefficient models (e.g. Flory–Huggins theory, etc.) or equations of state (EoS) (e.g. Sanchez-Lacombe equation of state–SL EoS, or perturbed-chain statistical associating fluid theory–PC-SAFT EoS). A schematic comparison of the equilibrium sorption behavior between the Henry's law, the SL EoS model, and PC-SAFT EoS model is presented in Figure 11.

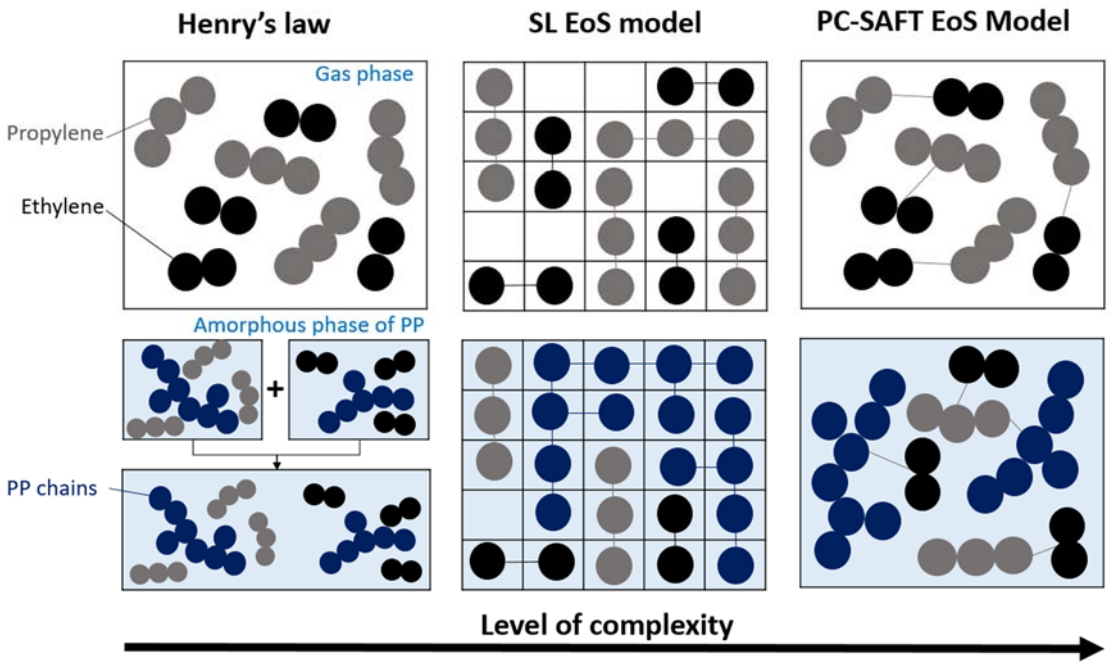

FIGURE 11 A schematic comparison between the Henry's law (sum of two individual ideal binary systems), the SL EoS, and PC-SAFT EoS models of the equilibrium sorption of the propylene and ethylene in amorphous polypropylene (PP) (a ternary system).

Henry's law

Henry's law, the simplest thermodynamic model, can be used to describe the sorption of monomer/commoner(s) in the amorphous phase of a semicrystalline polyolefin for an ideal gas system. The validity of Henry's law is limited to low concentrations (or low pressure) as monomer-polymer interactions may influence the gas solubility at high pressures. Stern et al.[89] proposed a Henry's law empirical correlation as a linear function of the ratio of the critical temperature of the penetrants to the actual temperature:

$$\log K^*_{\mathrm{H}_i} = A + B\left(\frac{T_{\mathrm{c},i}}{T}\right)^2 \quad (30)$$

where $K^*_{\mathrm{H}_i}$ is Henry's constant (mol/(atm L-amorphous)) of monomer i in the amorphous polymer; this parameter is independent of both pressure and volume fraction. $T_{\mathrm{c},i}$ is the critical temperature of the monomer i, T is the reaction temperature, and A and B are fitting parameters.

It should be noted that plasticizing effects due to penetrant sorption can occur above the gas critical properties (i.e. $P_{\mathrm{c},i}$, and $T_{\mathrm{c},i}$). The following expression, referred to as Stern's correlation,[89] was used to identify the condition at which pressures the Henry's law model begins to deviate by 5 % (P_{dev}):

$$\log\left(\frac{P_{\mathrm{dev}}}{P_{\mathrm{c},i}}\right) = 3.025 - 3.50\left(\frac{T_{\mathrm{c},i}}{T}\right) \quad (31)$$

Hutchinson and Ray[90] employed Stern's correlation to fit the parameters A and B using solubility data of different penetrants in semicrystalline polyethylene. Note however that the identified parameters are valid only for polyethylene. To the best of our knowledge, these parameters were not identified in the literature for polypropylene or its copolymers.

Thus, we used experimental gas solubility of propylene and ethylene in amorphous iPP at temperatures 50, 70, 85 °C from Cancelas et al.[91] to estimate the Henry's law solubility coefficients. Table 7 shows the parameters used in the Stern's correlation for polyethylene, and iPP.

TABLE 7 Summary of parameters used in Stern's correlation for the estimation of Henry's law constant ($K^*_{\mathrm{H}_i}$).

Systems		**Parameters used in Stern's correlation Equation (30)**		**Reference**
Polymer type	**Gas components**	**A**	**B**	
PE	α-Olefins ; H_2	-2.38	1.080	Hutchinson and Ray (1990) [90]

iPP	Propylene; Ethylene;	-2.315	1.307	This work using Cancelas et al. 's data[91]

At equilibrium, the concentration of a dissolved species in the amorphous polymer phase can then be calculated based on Henry's law (Equation (32))):

$$C_i^{\mathrm{p}} = K_{\mathrm{H}_i}^{*} P_i \tag{32}$$

Where P_i is the species *i* partial pressure in the vapor phase.

While Henry's law works reasonably well for single component solubilities, or solubities of mixtures with a dominant component, it is not able to account for the cosolubility effects should they be important.

PC-SAFT EoS model

The original SAFT EoS approach contains a sum of three molecular contributions; namely, reference, chain, and association contributions, to describe thermodynamic properties of the fluid mixtures,[92,93] The reference term accounts for the dispersive interactions which is a spherical segment (i.e., Lennard-Jones interactions), a hard sphere, or the square-well potentials. The chain term represents attractive interactions between the covalent chain-forming bonds among the segments. Finally, the association term accounts for hydrogen bonding and polar effects.[93]

Over the last few years, various versions of the SAFT EoS have been proposed and applied for chain-like molecules (i.e. polymer chains).[93] Among the modified SAFT EoS model, the PC-SAFT EoS model,[94] represents the latest modification of the SAFT EoS approach. The difference between the original SAFT and PC-SAFT models is that the attractive interactions in the SAFT model occur between individual molecules and chain segments, whereas the PC-SAFT model considers the attractive interactions between entire molecules (Figure 11). So, the hard-sphere fluid for the dispersion term was used in the original SAFT EoS model, while the hard-chain fluid was used in the PC-SAFT model, which is more realistic in describing the thermodynamic behavior of the chain-like fluid mixtures.

Modelling of the PC-SAFT requires three pure-component parameters for a nonassociating molecule: the segment number (m) corresponding to the deviation of the

molecules from the spherical shape, the segment diameter (σ), and the reduced interaction energy (ε/k) corresponding to the energy involved in the interaction between two segments. These parameters can be obtained by fitting to pure components data (i.e. vapor-pressure data) for the compounds of interest. To describe the binary and ternary mixtures, it is required to adjust the binary interaction parameters (k_{ij}) to correct for the deviations of the geometric mean of the energy parameter.[95] A full set of the PC-SAFT EoS expression as well as values of the three pure-component parameters can be found elsewhere.[94–96]

SL EoS model

The SL EoS is the extension of the well-known lattice theory of Flory and Huggins where the pure molecules are assumed to have one or more segments, and arrange randomly into a lattice structure (Figure 11). Unlike Flory−Huggins theory, the empty sites (or free volume) in the lattice are included in the SL EoS, thus allowing the model to account for compressibility and density effects due to volume changes.[97,98] The main equations of the SL EoS model equations can be found in the Supporting Informationsupplementary materials.

In the SL EoS model, the thermodynamic properties of the pure components can be characterized by three characteristic parameters, namely, characteristic temperature (T^*), characteristic pressure (P^*) and close-packed mass density (ρ^*). These parameters are generally available in the open literatures for a wide variety of gaseous penetrant species and polyolefins.[91,97–101] For the mixture systems, the characteristic interaction energy for the mixtures ($\varepsilon^*_{\mathrm{mix}}$), the characteristic closed-packed molar volume of a mer of the mixtures (v^*_{mix}), and the mixing rule for the number of sites (mers) occupied by a molecule of the mixture (r_{mix}) can be defined using the *"van der Waals"* mixing rule.

Similar to other equations of states, the SL EoS model relies on a binary interaction parameter (k_{ij}) which similarly can be identified based on experimental sorption data. A summary of the k_{ij} correlations found in the literatures for the binary– and ternary systems for both SL EoS is given in Table 8. It is important to point out that the presented k_{ij} correlation is only valid for the fitting experimental ranges.

TABLE 8 Summary of the thermodynamic modeling and binary interaction parameters used for binary- and ternary systems in propylene (co)polymerization.

System	Models	Binary Interaction Parameters (k*ij*)	Confidence interval	Reference
Binary system				
Ethylene(1)/iPP(2)	SL EoS	$k_{12} = -0.0003T + 0.0819$	T= [323; 343; 353] K; P= [0 - 25] bar; χ_{pol}= ◊53%	This work using data from Cancelas et al.[91]
Ethylene(1)/ICP(2)	SL EoS	$k_{12} = -0.0004T + 0.1961$	T= [323; 343; 363] K; P= [3.8 - 28.2] bar; χ_{pol}= *58.1%	This work using data from Sato et al.[102]
Propylene(1)/iPP(2)	SL EoS	$k_{12} = -0.0006T + 0.1987$	T= [323; 343; 353] K; P= [0 - 25] bar; χ_{pol}= ◊53%	This work using data from Cancelas et al.[91]
Propylene(1)/ICP(2)	SL EoS	$k_{12} = -0.0006\ T + 0.2251$	T= [323; 343; 363] K; P= [3.2 - 28.3] bar; χ_{pol}= *58.1%	This work using data from Sato et al.[102]
Ternary systems				
Ethylene(1)/ propylene(2)/ iPP (3)	SL EoS	$k_{12} = 0$ $k_{13} = -0.0003\ T + 0.0819$ $k_{23} = -0.0004\ T + 0.1463$	T= [323; 343; 353] K; P= [0 - 25] bar; χ_{pol}= ◊53%; $x_{C_3}: x_{C_2}$= 0.5:0.5	This work using data from Cancelas et al.[91]

Where χ_{pol} is the degree of crystallinity in mass (%)

*Crystallinities corresponding to polymer powder determined with X-ray diffraction (XRD)

+ Crystallinities corresponding to polymer powder determined with density method (bar sample)

◊Crystallinities corresponding to polymer powder determined with differential scanning calorimetry (DSC)

Previous studies have reported the use of EoS models to describe the thermodynamic behavior of various polymer-containing mixtures. Krallis and Kanellopoulos[99] employed the SL EoS and the PC-SAFT EoS to predict the physical and thermodymic properties in the catalytic olefin copolymerization systems over a wide range of pressures, temperature, and degree of polymer crystallinity. They concluded that both models can be used to describe the physical properties of the pure components and the thermodynamic properties. For the prediction of the pure component properties (i.e. vapor and supercritical density of monomer and comonomer(s)), the PC-SAFT EoS model provided better predictions. While, the SL EoS model provided excellent predictions of thermodynamic properties for binary systems (i.e. the solubility of ethylene in amorphous LLDPE-1-butene, the solubility of propylene in amorphous iPP, etc.) compared to the PC-SAFT EoS model. Alizadeh et al.[100] employed the SL EoS and PC-SAFT EoS models to predict the gas solubility of the binary systems – ethylene(1)/PE(2) and n-hexane(1)/PE(2) and the ternary system – ethylene(1)/n-hexane(2)/PE(3). They used the two thermodynamic models to investigate the effect of n-hexane as an ICA on the ethylene polymerization rate, so to account for the cosolubility effect. They concluded that both models are capable of describing the solubility of ethylene in the binary system of ethylene/PE. However, the SL EoS model provides higher accuracy for the description of the solubility of the ternary system of ethylene(1)/n-hexane(2)/PE(3) compared to the PC-SAFT EoS model. More recently, Mrad et al.[103] extended the SL EoS model to describe the thermodynamic properties of the quaternary system (monomer(1)/comonomer(2)/ICA(3)/polymer(4)). They also proposed a systematic procedure for the estimation of the SL interaction parameters used in the quaternary system. According to their studies, it is clearly seen that the nonideal interaction between different olefin components (ethylene, propane, and 1-butene) in the amorphous phase of PE cannot be neglected. Therefore, it is necessary to have thermodynamic data for at least the ternary system to be able to capture the co- and antisolvent effects in the polyolefin system.

General guidelines for the selection of suitable thermodynamic models

A systematic methodology to select the most appropriate thermodynamic models for catalytic olefin (co)polymerization is proposed in Figure 12. The objective is to avoid

unnecessary complicated time-consuming models but to capture physical phenomena (i.e. cosolubility and antisolubility) if they are relevant.

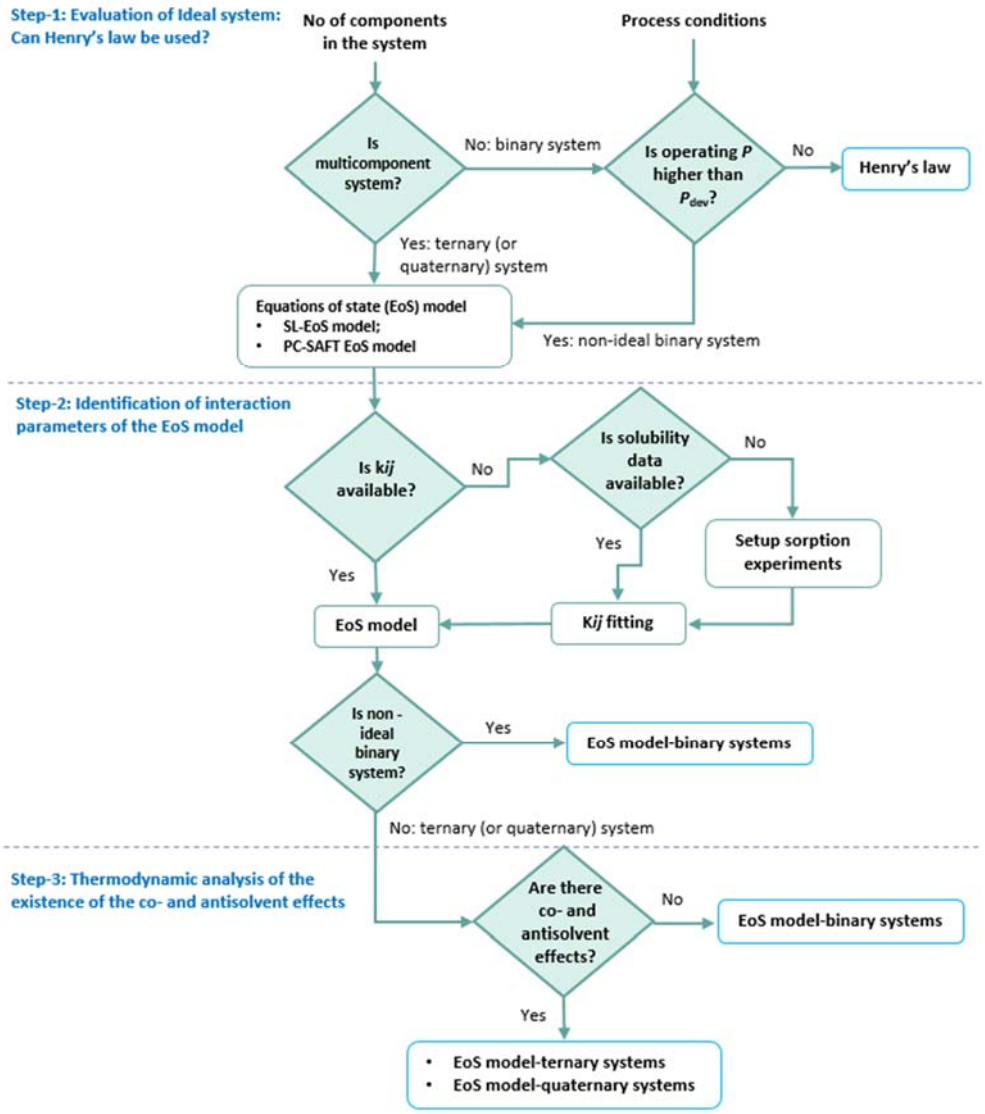

FIGURE 12 A general guideline for the selection of thermodynamic models for catalytic olefin (co)polymerization systems

To demonstrate the application of the proposed methodology for the selection of thermodynamic models the following case studies will be applied. Nevertheless, this methodology is flexible to apply for any gas phase olefin polymerizations of interest (e.g., α-olefins/LLDPE, α-olefins/HDPE, α-olefins/ICP, etc.). Both cases are operated under industrial conditions (25 bar and 70°C).

- Case study-1: propylene homopolymerization (to produce iPP)

- Case study-2: propylene-ethylene (equivalent mixture) copolymerization (to produce high ICP)

Step-1: Evaluation of ideal system: Can Henry's law be used?

With the given process conditions and recipes, one can identify if the system of interest is binary or of higher order. Case study-1 is a binary system as the system contains only propylene (1) and iPP (2). One can check further if this binary system can be assumed as an ideal gas system, and so to determine if we can use a simple Henry's law to estimate the equilibrium sorption of the monomer/commoner(s) in the amorphous polymer. Equation (31) can be used to calculate at which pressures (P_{dev}) the Henry's law cannot be used. For the case of propylene, the critical temperature, and pressure are 365.57 K, and 46.65 bar, respectively. Thus, P_{dev} of propylene at 70 °C is 9.23 bar. This means that the use of Henry's law to predict the propylene solubility in the amorphous iPP at pressure above 9.23 bar will be in error. It is suggested that beyond this pressure (the operating pressure at commercial scale is normally set between 25 to 30 bar), EoS models should be used to capture non-ideal behavior of the system.

Turning to case study-2 that is referred to ternary system of propylene(1)–ethylene(2)–iPP(3), there are 3 components in the systems. In this case, we have to evaluate if the effects of co- and antisolvent play a role using EoS model (SL-EoS model or PC-SAFT EoS model).

Steps 2 is required if we have a non-ideal binary system or a ternary (or quaternary) system.

Step-2: Identification of the interaction parameters of the EoS model:

In this step, it is crucial to have the interaction parameters in the available literatures (e.g. k_{13} and k_{23} for a ternary system) or gas solubility data (to identify these parameters) for the system of interest to analyze the impact of the co- and antsolvent effects.

The interaction parameters of the SL-EoS model for the propylene homo- and copolymerization (mostly to produce iPP and ICP) are given in Table 8 for a specific range of pressure and temperature. For case study-1 (propylene-iPP), it is referred to the non-ideal binary (pure component) system due to the high pressure of the system, thus the SL-EoS model with binary interactions is selected.

However, ternary solubility data of propylene and ethylene (8 % wt) in amorphous RCP is still missing. It is highly suggested to generate sorption data for this ternary system. For

ethylene (co)polymerization systems, the reader can find the interaction parameters in the available literature.[99,100,103–105]

Step-3: Thermodynamic analysis of the existence of the co- and antisolvent effects:

Steps 3 is required if we have a ternary (or quaternary) system.

In case study-2 (propylene-ethylene-iPP), in order to investigate the cosolubility effect of ethylene on propylene, and the antisolvent effect of propylene on ethylene in the amorphous iPP, one can compare between the two following ways: (a) a binary description (thus neglecting cosolubility and antisolubility effects of propylene and ethylene), and (b) a ternary description (propylene(1)/ethylene(2)/iPP(3)) that includes the effect of cosolubility and antisolubility.

Figure 13 compares the prediction of the solubility of propylene (1) and ethylene (2) (an equimolar mixture) in amorphous iPP using binary and ternary SL-EoS models. Both models (Figure 13a) give equivalent results over this range of pressure for the propylene, which means that the antisolvent effect of propylene on ethylene in the iPP is negligible. In this particular case, the use of SL EoS model with binary (pure component) interactions to predict multicomponent systems (propylene(1)/ethylene(2)/iPP(3)) would be recommended to reduce the computation time and model complexity.

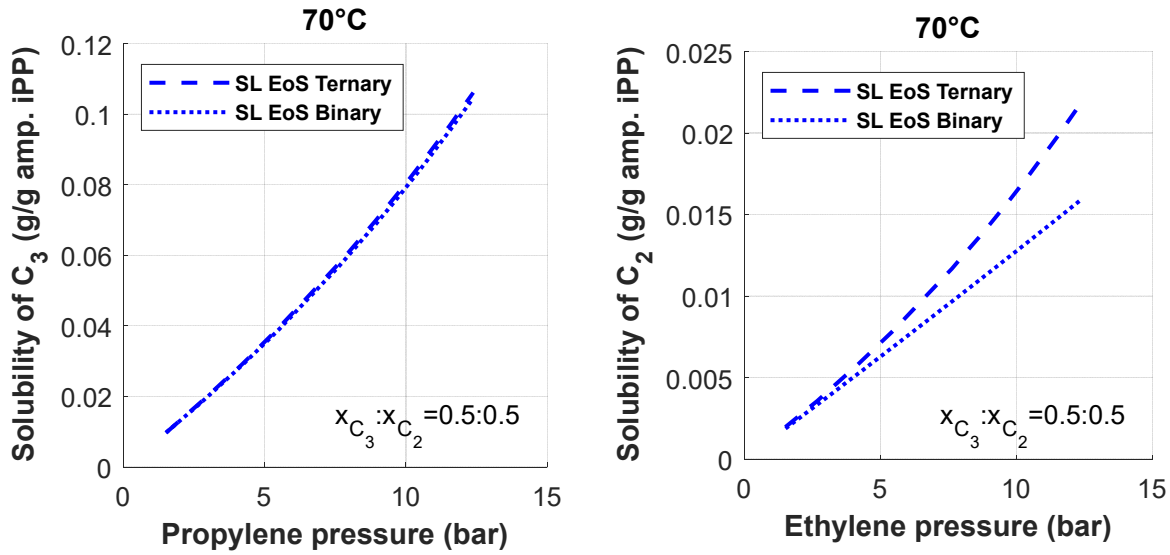

(a) (b)

FIGURE 13 Comparison of solubility of (a) propylene (b) and ethylene, (an equimolar mixture) in amorphous iPP at 70 °C predicted using binary and ternary models SL EoS.[91]

In Figure 13b, it can be seen that the solubility of ethylene in amorphous iPP using the SL EoS-ternary system is higher than in the binary SL EoS model. This is caused by the cosolubility effect in which the presence of the heavier component (i.e. propylene) enhances the solubility of the lighter gas (here ethylene) compared to the solubility of ethylene alone at the same operating conditions. For the prediction of ethylene solubility in amorphous PP copolymers (i.e. high ICP), it is necessary to use the SL EoS-ternary model to be able to account for the cosolubility and antisolvent effects. It is important to remind that the underprediction of the solubility of each component in amorphous polymer can lead us to under predict the gas concentration at the active site. This may significantly affect the rate of polymerization.

3.3.3 Diffusion models

Besides the solubility values used as boundary conditions in the SPM, the determination of diffusion coefficient is required in SPMs. Kanellopoulos et al.[83] proposed a model to estimate the overall effective diffusivity of a monomer in the semicrystaline polymer phase ($D_{i,\mathrm{eff}}$) as the function of the porosity of the particles and diffusivity coefficients:

$$D_{i,\mathrm{eff}} = \frac{\varepsilon^{\mathrm{p}}}{\tau^2} D_i^{\mathrm{g}} + (1-\varepsilon^{\mathrm{p}})(1+3\varepsilon) D_i^{\mathrm{pol}} \tag{33}$$

where τ is the tortuosity factor, ε^{p} the particle porosity, D_i^{g} the gas-phase binary diffusivity of the i^{th} species in a multicomponent gaseous system, estimated according to the gas diffusion theory of Chapman-Enskog,[106] and D_i^{pol} is the diffusivity of the i^{th} species in the amorphous polymer phase.

Alves et al.[104] proposed a model to calculate the diffusivity of the different species in the amorphous polymer while accounting for the codiffusivity effect. Indeed, a codiffusivity effect may occur in the presence of multiple gases, in analogy to the cosolubility effect. For example, in the polyethylene system in the presence of ICA, the diffusivity of both ethylene and ICA is affected by the presence of the other species.[104] Ben Mrad et al.[107] recently estimated the diffusion coefficient of different gas species in amorphous PE in multi-component systems using a magnetic suspension balance, and observed a codiffusivity effect in most cases. For more details on this topic, the reader may refer to the above mentioned papers; this will not be discussed here.

3.4 Macroscale: Reactor level

This section will discuss the general model assumptions and conservation equations used to model gas phase multi-volume polymerization reactors, particularly the MZCRs, while modelling single zone reactor type, such as FBR and VSBR, is beyond the scope of this paper. A review of FBR and VSBR models can be found in references.[27,108–113] The focus in this section will be on the reactor model. The reaction rate calculation (R_j) in the references discussed here can be different from Table 6 (e.g. some reaction mechanisms were simplified), but we will not report or discuss their models of R_j.

3.4.1 MZCR modelling

Few attempts have been made to develop mathematical models of the MZCR, starting from existing models of single zone models. Fernandez and Lona[43,44] firstly developed an isothermal, steady state model of the MZCR for PE production with and without a barrier gas, and performed a parameter sensitivity analysis of the operating conditions (i.e. the catalyst flow rate, monomer and inert concentrations, gas velocity in the riser, riser bed porosity, and bed height in the downer) on the reactor behavior (i.e. production rate and polymer product characteristics, e.g. instantaneous $\bar{M}_w$). Ghasem et al.[46,47] extended the proposed steady state model of Fernandez and Lona to a non-isothermal dynamic model, so that the transient behavior of the MZCR could be investigated.

Santos et al.[16,17] firstly developed an isothermal and dynamic mathematic MZCR model for propylene homo- and copolymerization. They considered a multiscale model including the macroscale level (reactor modeling), the mesoscale level (single particle modelling), and the microscale level (a simplified kinetic modelling, neglecting the catalyst site deactivation, and the effects of hydrogen responses ─ by the formation and reactivation of dormant site reactions). The effects of mass transfer limitations on particle growth were investigated using the MGM model. The proposed model was capable of predicting the polymer productivity, particle size distribution (PSD), average molecular weights (i.e. $\bar{M}_w$ and $\bar{M}_n$) and polydispersity of the final polymer particles. Nonetheless, there was no clear explanation on how to transfer information between the sub-models (i.e. input information transferred from the particle model to the reactor model). Furthermore, Henry's law was used to predict the solubility, so neglecting non-ideal behaviors and the co- and antisolvent effects.

Adli et al.[45] improved the steady-state model of Fernandez by treating the moving solid particles as clusters rather than individual particles, in the case of ethylene copolymerization.

They made it clear that the formation of clusters highly influences the hydrodynamics and cannot be neglected in the MZCR. Indeed, the cluster velocity and the bed porosity are not constant along the riser length, and they change upon the hydrodynamic zones (i.e. a lower dense zone, an acceleration and fully developed zone, and a deceleration zone). However, according to the moving packed bed nature of the downer, the cluster velocity and the bed porosity are fairly constant in fully developed zones. The authors argued that their model could describe more realistic hydrodynamics of the MZCR behaviors.

Considering the CFD works on the MZCR, Wei et al.[114] used CFD to study gas–solid flow dynamics in a propylene polymerization MZCR and investigate the effect of exit configuration of the riser. Yan et al.[115] improved Wei et al. work by coupling the CFD model with a population balance model to capture the effect of polydisperse particles inside the MZCR. A simplified kinetic scheme (i.e. propagation reaction) of the propylene polymerization was incorporated to estimate the temperature profiles in the MZCR. Yan et al.[116] took benefits of the CFD for designing a gas barrier inlet configuration for a MZCR. More recently, Marandi and co-workers[117] used a 3D CFD model for simulating the hydrodynamics of polypropylene powders in the MZCR. The proposed model was used to design a proper geometry of the reactor with the best operating conditions from the hydrodynamic point of view.

General assumptions used in the development of the MZCR model presented below are the following:

- Prepolymerized catalyst is introduced continuously at the bottom of the riser;
- Fluid flow patterns of the gas and polymer particles in the riser and the downer can be described by a plug flow model.
- The solid particles are assumed to move as individual particles. Particle aggregation and breakage are negligible;
- Internal mass transfer within the particles is negligible, so thermodynamic equilibrium is reached quickly (so we will not include an SPM here; please refer to section 3.3 to include it);
- A two-phase model is considered in the reactor: gas phase (monomer, comonomer, and inerts), and solid phase (polymer particles). Both phases will be assumed to have the same temperature but different velocities;
- In the riser, the hydrodynamic regime follows the principles of pneumatic transport under fast fluidizing condition, where the net velocity of the particle (u_s^R) is calculated

as the difference between the upward gas velocity ($u_{\mathrm{g}}^{\mathrm{R}}$) and the terminal (or equilibrium) velocity (u_{t}); [16,17,118]

- The cyclone is assumed to be working perfectly allowing all the particles coming from the riser to go to the downer (no loss of small particles);
- Throughout the downer, the gas-solid relative velocity ($u_{\mathrm{s}}^{\mathrm{D}} - u_{\mathrm{g}}^{\mathrm{D}}$) must be lower than the minimum fluidization ($u_{\mathrm{mf}}^{\mathrm{D}}$) in order to ensure a packed moving bed condition [16,17] and the bed porosity is assumed to be constant in the downer;

$$u_{\mathrm{mf}}^{\mathrm{D}} \geq \left| u_{\mathrm{s}}^{\mathrm{D}} - u_{\mathrm{g}}^{\mathrm{D}} \right| \tag{34}$$

The conservation equations of mass, momentum, and energy balances of the MZCR are shown in Table 9. The boundary conditions used for the development of the MZCR modelling is presented in Table 10.

TABLE 9 Summary of conservation equations (mass, momentum, and energy balances) used for the development of the MZCR model for propylene copolymerization[a].

Mass balances	**Conservation equations**	**Equation**
Continuity equations of total gas (kg m^{-3}_{void})[16]	$\frac{\partial \rho_{\mathrm{g}}}{\partial t} = -\frac{\partial \rho_{\mathrm{g}} u_{\mathrm{g}}}{\partial z} - \frac{1}{\varepsilon^{\mathrm{bed}}} \sum_{i=1,2,\mathrm{H_2}} R_i M_{\mathrm{w},i}$	(35)
Mass balances of gas species (-)[16]	$\frac{\partial w_i}{\partial t} = -u_{\mathrm{g}} \frac{\partial w_i}{\partial z} + \frac{R_i M_{\mathrm{w},i}(w_i - 1)}{\rho_{\mathrm{g}} \varepsilon^{\mathrm{bed}}} + \frac{1}{\rho_{\mathrm{g}} \varepsilon^{\mathrm{bed}}} w_i \sum_{l \neq i} R_l M_{\mathrm{w},l}$ $\frac{\partial w_{\mathrm{Inert}}}{\partial t} = -u_{\mathrm{g}} \frac{\partial w_{\mathrm{Inert}}}{\partial z} + \frac{1}{\rho_{\mathrm{g}} \varepsilon^{\mathrm{bed}}} w_{\mathrm{Inert}} \sum_{i=1,2,\mathrm{H_2}} R_i M_{\mathrm{w},i}$ Where *i:* 1, 2, H_2	(36) (37)
Mass balances of solid species (mol m^{-3}_{bed})[16]	$\frac{\partial C_j}{\partial t} = -\frac{\partial C_j u_{\mathrm{s}}}{\partial z} + R_j$	(38)
Momentum balances		
Conservation of momentum for the gas phase (m s^{-1})[16]	Riser: $\frac{\partial u_{\mathrm{g}}^{\mathrm{R}}}{\partial t} = -u_{\mathrm{g}}^{\mathrm{R}} \frac{\partial u_{\mathrm{g}}^{\mathrm{R}}}{\partial z} + \frac{u_{\mathrm{g}}^{\mathrm{R}}}{\rho_{\mathrm{g}}^{\mathrm{R}} \varepsilon^{\mathrm{R}}} \sum_{i=1,2,\mathrm{H_2}} R_i^{\mathrm{R}} M_{\mathrm{w},i} - \frac{F^{\mathrm{R}}}{\rho_{\mathrm{g}}^{\mathrm{R}}} - \mathrm{g} -$ $\frac{\mathrm{RT}}{\rho_{\mathrm{g}}^{\mathrm{R}}} \frac{\partial \rho_{\mathrm{g}}^{\mathrm{R}}}{\partial z} \sum_{i=1,2,\mathrm{H_2},\mathrm{Inert}} \left(\frac{w_i^{\mathrm{R}}}{M_{\mathrm{w},i}} \right) -$ $\mathrm{RT} \sum_{i=1,2,\mathrm{H_2},\mathrm{Inert}} \left(\frac{1}{M_{\mathrm{w},i}} \frac{\partial w_i^{\mathrm{R}}}{\partial z} \right)$	(39)

	Downer: $\frac{\partial u_{\mathrm{g}}^{\mathrm{D}}}{\partial t} = -u_{\mathrm{g}}^{\mathrm{D}} \frac{\partial u_{\mathrm{g}}^{\mathrm{D}}}{\partial z} + \frac{u_{\mathrm{g}}^{\mathrm{D}}}{\rho_{\mathrm{g}}^{\mathrm{D}} \varepsilon^{\mathrm{D}}} \sum_{i=1,2,\mathrm{H}_2} R_i^{\mathrm{D}} M_{\mathrm{w},i} - \frac{F^{\mathrm{D}}}{\rho_{\mathrm{g}}^{\mathrm{D}}} + \mathrm{g} -$ $\frac{\mathrm{RT}}{\rho_{\mathrm{g}}^{\mathrm{D}}} \frac{\partial \rho_{\mathrm{g}}^{\mathrm{D}}}{\partial z} \sum_{i=1,2,\mathrm{H}_2,\mathrm{Inert}} \left(\frac{w_i^{\mathrm{D}}}{M_{\mathrm{w},i}} \right) -$ $\mathrm{RT} \sum_{i=1,2,\mathrm{H}_2,\mathrm{Inert}} \left(\frac{1}{M_{\mathrm{w},i}} \frac{\partial w_i^{\mathrm{D}}}{\partial z} \right)$ F^{R} and F^{D} describe for the friction losses in each reactor (see equations 14S-18S in Supporting Information).	(40)
Conservation of momentum for the solid phase (m s^{-1})[16]	Riser: $u_{\mathrm{s}}^{\mathrm{R}} = u_{\mathrm{g}}^{\mathrm{R}} - u_{\mathrm{t}}$ u_{t} is the terminal velocity of spherical particles (see equations 10S in Supporting Information). Downer: $\frac{\mathrm{d}u_{\mathrm{s}}^{\mathrm{D}}}{\mathrm{d}z} = \frac{1}{\rho_{\mathrm{pol}}(1-\varepsilon_{\mathrm{pol}})} \sum_{i=1,2} R_i^{\mathrm{D}} M_{\mathrm{w},i}$	(41) (42)
Energy balances		
Conservation of Energy (K)[43] for riser and downer	$\frac{\mathrm{d}T^{\mathrm{bed}}}{\mathrm{d}z} =$ $- \frac{(-\Delta H_{\mathrm{rxn}}) \sum_{i=1,2,\mathrm{H}_2} R_i^{\mathrm{bed}} M_{\mathrm{w},i}}{\left[u_{\mathrm{g}}^{\mathrm{bed}} \sum_{i=1,2,\mathrm{H}_2} (C_{\mathrm{p}i} C_i^{\mathrm{bed}} M w_i) \varepsilon^{\mathrm{bed}} + u_{\mathrm{s}}^{\mathrm{bed}} (1-\varepsilon^{\mathrm{bed}}) C_{\mathrm{p,pol}} \rho_{\mathrm{s}}\right]}$	(43)

[a] Superscript R is riser, D is downer and bed is reactor (so can be both R or D); Subscript i, l is 1: propylene, 2: ethylene, H_2: hydrogen, and Inert: propane; Subscript j refers to all solid species including catalyst and moments (i.e. P_0, λ_0, λ_1, λ_2, μ_0, μ_1, μ_2), (if R_i is in mol m^{-3}_{bed} s^{-1}).

The bed porosity in the riser (ε^{R}) is calculated by deducing the volume of polymer particles which is calculated by integrating the PSD (from the population balance, Equation ((44)). According to the simulation results of Santos et al.,[16,17] the bed porosity slightly decreases along the riser height from the bottom to the top, as the amount of solid polymer increases due to the polymerization reaction. In the downer, the bed porosity is constant over space ($\varepsilon^{\mathrm{D}} = 0.35$)[17] due to the moving packed bed behavior of the downer.

$$\varepsilon^{\mathrm{R}} = 1 - \int_{v_0}^{\infty} q_{\mathrm{n}}^{\mathrm{R}}(z,v)v\mathrm{d}v \tag{44}$$

Where $q_{\mathrm{n}}(z,v)$ is the particle density function in number per bed volume per volume of particles (part m^{-3}_{s} m^{-3}_{bed}) determined by the following population balance equation (neglecting particle aggregation and breakage):

$$\frac{\partial q_{\mathrm{n}}(z,v)}{\partial z} = -\frac{G_{\mathrm{p}}}{u_{\mathrm{s}}}\frac{\partial q_{\mathrm{n}}(z,v)}{\partial v} - \frac{q_{\mathrm{n}}(z,v)}{u_{\mathrm{s}}}\frac{\partial u_{\mathrm{s}}}{\partial z} \tag{45}$$

The volumetric growth rate of particles (G_{p}, m^3 s^{-1}) is given by:

$$G_{\mathrm{p}} = \frac{\sum_{j=1}^{\mathrm{NC}} M_{\mathrm{w},j}R_j}{N_{\mathrm{p}}\rho_{\mathrm{pol}}(1-\varepsilon_{\mathrm{pol}})} \tag{46}$$

Note that the growth rate is dependent on the height z. The total number of particles per bed volume is given by:

$$N_{\mathrm{p}} = \int_{v_0}^{\infty} q_{\mathrm{n}}(z,v)\mathrm{d}v \tag{47}$$

3.4.2 FBR-IC modelling

As mentioned in Section 2.2.2, the FBR-IC can be divided into three sections (Figure 5): the draft tube, the annulus and the cone.

Meier et al.[34] originally developed a compartment model of the FBR-IC to describe the concentration and temperature profiles inside the reactor and the polymer properties (e.g. MWDs). In their model, the draft tube and annulus zones were divided into several compartments configured in series, where each compartment was modelled as a CSTR (so N CSTRs in series), to simulate the plug-flow like behavior of the reactor (Figure 14), while the cone was assumed as one CSTR. In this approach, one must identify the number of CSTRs (N) beforehand, and the input and output parameters of each compartment, which is particularly difficult to know. According to their findings, the particle circulation rate was strongly influenced by the reactor geometry (i.e. length and diameter of the draft tube, the angle of the cone, and the distance between the draft and the cone). They used the developed model to study the influence of the gas velocity on the particle circulation rate.

In this section, we will consider modelling both the draft tube and annulus sections as a PFR and model the cone as a CSTR (Figure 5b).

TABLE 10 Boundary conditions (for $t > 0$) and initial conditions (for $0 \le z \le L$) used for the development of the MZCR modelling for propylene copolymerization[a,b,c] [16,17].

Parameters	The riser model	Equation	The downer model	Equation
Gas density	$\rho_g\|^{R}_{z=0} = \rho_g^{R,fresh}$ $\rho_g\|^{R}_{t=0} = \rho_g^{R,fresh}$	(48) (49)	$\rho_g\|^{D}_{z=0} = \rho_g^{D,fresh}$ $\rho_g\|^{D}_{t=0} = \rho_g^{D,fresh}$	(50) (51)
Gas mass fractions	$w_i\|^{R}_{z=0} = w_i^{R,fresh}$ $w_i\|^{R}_{t=0} = w_i^{R,fresh}$	(52) (53)	$w_i\|^{D}_{z=0} = w_i^{D,fresh}$ $w_i\|^{D}_{t=0} = w_i^{D,fresh}$	(54) (55)
Solid concentrations	$C_j\|^{R}_{z=0} = \frac{(1-\varepsilon^{R,in})}{(1-\varepsilon^{D})}\phi_{rec}C_j\|^{D}_{z=L}$ $C_j\|^{R}_{t=0} = 0$ $C_{P_0}\|^{R}_{z=0} = \frac{(1-\varepsilon^{R,in})}{(1-\varepsilon^{D})}\phi_{rec}C_{P_0}\|^{D}_{z=L} + \frac{(1-\varepsilon^{R,in})}{(1-\varepsilon^{prep})}\phi_{prep}C_{P_0}^{prep}$ $C_{P_0}\|^{R}_{t=0} = C_{P_0}^{prep}$	(56) (57) (58) (59)	$C_j\|^{D}_{z=0} = \frac{(1-\varepsilon^{D})}{(1-\varepsilon^{R})} C_j\|^{R}_{z=L}$ $C_j\|^{D}_{t=0} = 0$	(60) (61)
Particle density function	$q_n^R\|^{v}_{z=0} = \frac{(1-\varepsilon^{R,in})v q_n^{tot}}{\int_{v_0}^{\infty} q_n^{tot} v dv}$, $q_n^{tot} = \frac{1}{(1-\varepsilon^{prep})}\phi_{prep}q_n^{prep} + \frac{1}{(1-\varepsilon^{D})}\phi_{rec}q_n^D\|^{D}_{z=L}$	(62) (63)	$q_n^D\|^{v}_{z=0} = q_n^R\|^{v}_{z=L}\frac{(1-\varepsilon^{D})}{(1-\varepsilon^{R})}$	(64)
Bed porosity at the entry	$\varepsilon^{R,in} = \frac{Q^R}{2S_r^R u_t} - \frac{1}{2}\sqrt{\left(\frac{Q^R}{S^R u_t}\right)^2 - \frac{4u^{R,in}\varepsilon^{R,in}}{u_t}}$ $Q^R = u_t S^R + u^{R,in}S^R\varepsilon^{R,in} + Q_s^{rec} + Q_{prep}$	(65) (66)	$\varepsilon^{D} = 0.35$	(67)

[a] subscript i is 1 : propylene, 2: ethylene, H_2: hydrogen, and inert: propane.

[b] subscript j refers to all solid species (moments, catalyst, etc.) except potential active sites that are injected from the downer as well as from fresh prepolymer feed.

[c] $\phi_{rec} = \frac{Q_s^{rec}}{Q_s^{rec}+Q_{prep}}$; $\phi_{prep} = \frac{Q_{prep}}{Q_s^{rec}+Q_{prep}}$

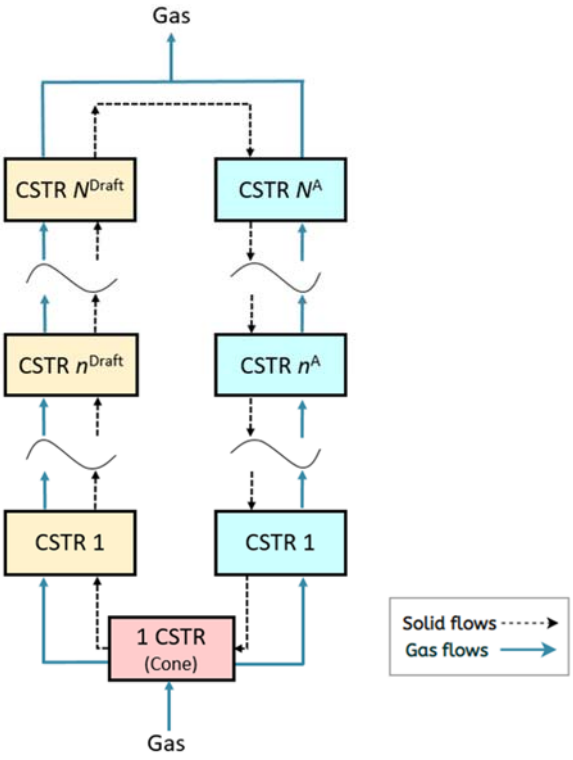

FIGURE 14 A schematic diagram of the FBR-IC model as *N* CSTRs in series, adapted from Meier et al.[34]

General assumptions for the FBR-IC model given in Table 11[34] are summarized below:

1. The draft tube and annulus sections are modelled as PFRs, whereas the cone section is modelled as a CSTR (Figure 5b);
2. The mass and heat transfer resistances between the gas and solid are negligible (so thermodynamic equilibrium is assumed and no SPM will be used, but it can be added without any restriction);
3. The growing polymer particles circulating in the system are continuously absorbing and desorbing propylene due to the temperature gradients between the sections;
4. Temperature distribution in the draft tube section is uniform, and different from the annulus section.
5. The velocity of the gas and solids in the reactor are uniform;
6. The bed porosity of the cone and draft tube sections is the same, and constant (0.75),[34] whereas the annulus section is a moving packed bed with a lower porosity (also constant, 0.44);[34]
7. There is no particle breakage or agglomeration in the model presented below (but these terms may be added without any restriction);
8. There is no heat transfer between the annulus and the draft tube section;

The conservation equations of mass, momentum, and energy balances of the FBR-IC are shown in Table 11. The initial and boundary conditions of the FBR-IC modelling can be analogous to the MZCR model presented in Table 10.

3.4.3 HSBR modelling

Many reactor modelling studies of the HSBR[38,39,42,49,113,119] focused on the prediction of the RTD of the polymer powder as it can affect the PSD and the distributions of the polymer properties such as particle compositions, and MWDs. Khare et al.[50] proposed a steady-state and dynamic reactor model to predict the polymer production rate, average molecular weight, and grade transitions by considering reactor mass holdup as the simulation target instead of the RTD. Kouzai and Fukuda[120] developed a reactor model that includes the effect of liquid propylene polymerization to study more realistic polymerization environment.

Several researchers used the concept of a number of equivolume CSTRs in series[38,39,42,49,50,113] to describe the RTD of the HSBR. Caracotsios[38] suggested that the RTD of the polymer powder produced in the HSBR is equivalent to that made by three to five equivolume CSTRs in series but each CSTR is with a different mean residence time. They found that the predicted polymerization yield depends on the number of the CSTRs (N) and the catalyst feed configuration pattern. It is common knowledge that the more CSTRs are added to the sequence, the narrower the reactor RTD, which would approach that of a PFR.[121]

In the HSBR, the catalyst is fed at the front end of the reactor, moves through the reactor, and reacts with the reacting gas in each reaction zone forming growing polymer particles in each stage to the rear end of the reactor. This means that the cumulative polymer overflow keep increasing from zone to zone, thus monotonically decreasing the mean residence time.[113] The exit age distribution function at the N^{th} CSTR (for fully backmixed CSTRs in series with equivalent volumes) can be obtained by the convolution of the RTD of each reactor.[38,49]

$$E(t) = \sum_{i=1}^{N} \frac{\tau_i^{N-2}}{\prod_{j=1, i\neq j}^{N}(\tau_i - \tau_j)} \exp(-\frac{t}{\tau_i}) \quad (68)$$

Where $E(t)$ is the exit age distribution function (s^{-1}), t is the residence time (s), τ is the mean residence time (s), and N is the total number of the CSTRs.

TABLE 11 Summary of conservation equations (mass, momentum, and energy balances) used for FBR-IC modelling of propylene polymerization.

Parameters	**Cone model**[34]	**Equation**	**Draft tube model**[16,17] (Similar to the Riser)	**Annulus model**[16,17] (Similar to the Downer)
Reactor model	1 CSTR		1 PFR	1 PFR
Continuity equations of total gas	-	-	Equation (35)	Equation (35)
Mass balances of gas species i (-)	$\frac{\mathrm{d}(V^{\mathrm{C}}\varepsilon^{\mathrm{C}}\rho_{\mathrm{g}}w_i^{\mathrm{C}})}{\mathrm{d}t} = \varepsilon^{\mathrm{C}}u_{\mathrm{g,in}}A^{\mathrm{C}}\rho_{\mathrm{g}}\left(w_{i,\mathrm{in}}^{\mathrm{C}} - w_i^{\mathrm{C}}\right) - V^{\mathrm{C}}R_i^{\mathrm{C}}Mw_i$	(69)	Equation (36)	Equation (36)
Material balances of solid species j (mol m^{-3}_{bed})	$\frac{\mathrm{d}C_j}{\mathrm{d}t} = \frac{F_j}{(1-\varepsilon^{\mathrm{C}})V^{\mathrm{C}}\rho_{\mathrm{s}}}\left(C_{j,\mathrm{in}} - C_j\right) + R_i^{\mathrm{C}}$	(70)	Equation (38)	Equation (38)
Conservation of momentum for the gas phase (m s^{-1})	-	-	Equation (39)	Equation (40)
Conservation of momentum for the solid phase (m s^{-1})	-	-	Equation (41)	Equation (42)
Energy balances (J s^{-1})	$\frac{\mathrm{d}(V^{\mathrm{C}}\bar{\rho}^{C}\bar{C}_p^{\mathrm{C}}T^{\mathrm{C}})}{\mathrm{d}t} = \sum_{i=1,\mathrm{H2}} F_{\mathrm{g}i}^{\mathrm{C}}C_{pi}(T_{i,\mathrm{in}}^{\mathrm{C}} - T^{\mathrm{C}}) + F_{\mathrm{s}}^{\mathrm{C}}C_{p,\mathrm{pol}}\left(T_{\mathrm{s,in}}^{\mathrm{A}} - T^{\mathrm{C}}\right) + (-\Delta\mathrm{H}_{\mathrm{rxn}})V^{\mathrm{C}}\sum_{i=1,2,\mathrm{H}_2} R_i^{C}M_{\mathrm{w},i}$	(71)	Equation (43)	Equation (43)

Where F_j is the mass flow rate of solid component j (kg s^{-1}), C_{pi} is the specific heat of component i in J kg^{-1} K^{-1}, ΔH_{rxn} is the polymerization reaction heat in J kg^{-1}, and R_i is in mol m^{-3}_{bed} s^{-1}). Subscript i is 1 : Propylene, and H_2: Hydrogen. Subscript j is S_p and P_0 and superscript C is cone section.

Gorbach et al.[113] developed a dynamic model of the HSBR to predict the production rate and the RTD. Dittrich and Mutsers[39] proposed four different solid flow models that include backmixing effects between each two connecting reactors to describe the RTD and powder flow pattern in the HSBR. Two types of models were proposed, a simple and a more complex overflow pattern (or backflow model). The simple overflow pattern model, is constituted of 4 CSTRs in series, and was defined as the net flow that moves from one CSTR to the following one with equivalent residence time (Model A, Figure 15) and with equivalent volume (Model B). Thus, only the number of CSTRs (N^{th}) was used as an adjustable parameter to describe the experimental RTD. The backflow models (models C and D) were built as cascades of more CSTRs (8-12 CSTRs in series) with axial net flow and forth- and backmixing flows caused by agitator rotation (see Figure 15). In this case, the number of the CSTRs in series was set beforehand, and the backmixing flow rate (F_m) was used as a tuning parameter to fit the experimental RTDs. They concluded that only the backflow model (i.e. model C and D) were suitable to characterize the RTD of the powder inside the HSBR. The basic equations used to develop the backflow model equations (model C) is shown in Table 12.

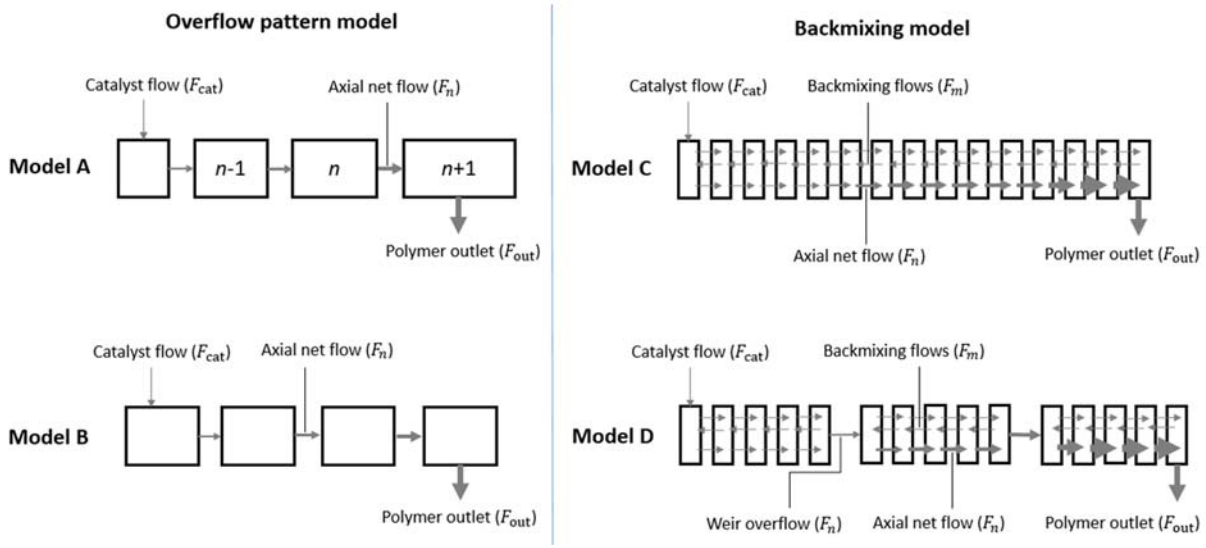

FIGURE 15 Illustration of the solid flow models for the HSBR proposed by Dittrich and Mutsers[39]. Flow model A and B are the simple overflow model, Flow model C and D are the backflow model. Adapted from Dittrich and Mutsers[39].

General basic assumptions of the HSBR model presented below are as follows:[39]

1. Catalyst is added continuously at the front of the reactor and mixed uniformly with solid polymer;
2. The monomer dissolved in the polymer powder at the outlet of the reactor is neglected;
3. The model is considered to have two phases: (1) the gas phase is assumed to be well-mixed, (2) the solid phase (polymer power) behaves as if it is moving through *N* CSTRs in series;
4. The volume of each reaction zone is equivalent, thus the mean residence time of each reaction will steadily decrease from one reaction zone to the next one, to reflect the accumulation of polymer yield;[49]
5. The temperature and pressure of all reaction zones are the same;
6. There is no particle breakage or agglomeration in the PBE presented below, but this can be added without restriction;
7. The internal mass transfer, and its limitations are negligible, so thermodynamic equilibrium is considered and no SPM is used, but this can be added without restriction;

TABLE 12 A summary of the backflow model equations (model C) proposed by Dittrich and Mutsers[a].[39]

Mass balances	**Model equation**	**Equation**
Total solid mass balance for each CSTR *n* (kg s^{-1})	$\frac{dm^n}{dt} = (F^{n-1} - F^n) + V^n \sum_j R_j^n M_{w,j}$ Where m^n is the ratio of the total solids mass hold-up in the HSBR (kg) to the number of the CSTRs in series (*N*) given by: $m^n = \frac{m}{N}$ F^n is the outlet mass flow rate of CSTR *n* (kg s^{-1}), R_j^n is the reaction rate of the solid component *j* (mol m^{-3}_{bed} s^{-1}), V^n is the volume of the CSTR *n* (m^3).	(72) (73)

Mass balances	Model equation	Equation
Mass balance of solid species j in each CSTR kg s^{-1})	$\frac{\mathrm{d}(w_j^n m^n)}{\mathrm{d}t} = w_j^{n-1}(F^{n-1} + F_m) - w_j^n(F^n + 2F_m) + w_j^{n+1}F_m + V^n R_j^n M_{\mathrm{w},j}$ Where w_j^{n} is the mass fraction of solid species j in each CSTR n. F_m is the backmixing mass flow rate at the boundary of the connecting CSTRs given by: $F_m = \frac{F(\sigma_0^2 N - 1)}{2}$ Where F is the throughput in the reactor (kg s^{-1}), σ_0^2 is the relative variance of the RTD given by $\sigma_0^2 = \tau^{-2} \int_0^\infty (t-\tau)^2 E(t)\mathrm{d}t$ Note that this relationship is suitable for a system with less backmixing (i.e. Bodenstein number > 100)	(74) (75) (76)
Batch polymer yield (γ_{pol}^k) at site k ($\mathrm{kg_{pol}\,kg^{-1}_{cat}}$)	$\gamma_{\mathrm{pol}}^k = \frac{P_{\mathrm{C_3}} k_{\mathrm{a}}^k k_{\mathrm{p}}^k}{k_{\mathrm{d}}^k - k_{\mathrm{a}}^k} \left\{ \frac{1-\exp(-k_{\mathrm{a}}^k t)}{k_{\mathrm{a}}^k} - \frac{1-\exp\left(-k_{\mathrm{d}}^k t\right)}{k_{\mathrm{d}}^k} \right\}$ It is assumed two-site catalysts (i.e. k = 2) and the kinetic parameters (i.e. k_{a} (s^{-1}), k_{p} ($\mathrm{kg_{pol}\,kg^{-1}_{cat}\,Pa^{-1}\,s^{-1}}$), and k_{d} (s^{-1})) are constant during the whole catalyst lifetime in the HSBR. Where k_{a}^k is activation constant of site k, k_{d}^k is deactivation constant of site k, k_{p}^k propagation constant of site k, and $P_{\mathrm{C_3}}$ is the partial pressure of propylene (Pa)	(77)
PSD of the particle (d_{pol}) (m)	$d_{\mathrm{pol}} = d_{\mathrm{cat}} \sqrt[3]{1 + \frac{\rho_{\mathrm{cat}}}{\rho_{\mathrm{pol}}} \sum_{k=1}^{2} \gamma_{\mathrm{pol}}^k}$ Where d_{cat} is the diameter of the catalyst, ρ_{cat} and ρ_{pol} is the density of the catalyst, and the polymer, respectively	(78)

[a]Subscript j is solid species (potential, active and dead catalysts, and polymer), superscript n is the index of the CSTR in series (n = 1, … , *Nth*)

4 CURRENT CHALLENGES AND IMPORTANT ISSUES FOR THE PP GAS PHASE MULTIZONE REACTOR MODELLING

Before discussing the conclusions and current challenges for PP modeling we need to perhaps think a little bit about model complexity. One should not confound complexity and multiscale, nor should we automatically opt for the most complex representation possible. To state the obvious, more complex models give one a more detailed understanding of the system under study. On the other hand, if there is no need for such detailed understanding, it is probably sufficient to use a model with reduced complexity. For instance, if we simply wish to know how changing the feed composition to an FBR impacts the productivity, it is probably reasonable to use an isothermal CSTR representation of the reactor, no single particle model (i.e. assume no heat and mass transfer resistances at the particle level), and an approximate microscale model:

$$\mathrm{R_p} = k_p^{\mathrm{lump}} C^* C_i^{\mathrm{p}} \tag{79}$$

where k_p^{lump} is a lumped propagation coefficient, C^* is the total concentration of active sites in the catalyst particles and C_i^{p} is the equilibrium concentration of monomer in the amorphous phase. So even for such a simplified problem solution, we still need a (simple) microscale model, a thermodynamic model at the mesoscale and the CSTR RTD model at the macroscale. In other words, we still need to consider the different length scales in our model. This means of course that modelling presents many challenges at the different scales as well as the connection between these scales, regardless of the complexity of the model.

Nevertheless, we often need to have a much more detailed picture of the polymerization process and the polymer properties, therefore imposing the need for a complex, detailed multiscale model. From this review we can clearly see of olefin polymerization processes, including PP processes, are quite complex, with many important physical and chemical phenomena that require much deeper understanding.

4.1 Microscale

4.1.1 Kinetics

The microscale includes both kinetic phenomena, as well as the growth and properties of the polymer chains. As we have seen above, a kinetic model for olefin polymerization has many

individual steps (activation, propagation, transfer, etc.) that can occur simultaneously. ZN catalysts (or Chromium catalysts which are not discussed here as the review focused on PP processes) also have multiple active catalyst sites, where each active site has its own set of kinetic constants for each of the many reaction steps.

One can identify several questions related to kinetic modelling, including:

- Is our understanding of the kinetic mechanism provided above correct? It appears that this kinetic mechanism allows us to model a great deal of what we observe experimentally, so in this sense it is accurate. However there remain a certain number of grey zones. In the particular case of PP, it appears that the catalysts are much more thermally sensitive than similar catalysts used for PE. Heating a PP catalyst with both internal and external donors can clearly lead to a significant deactivation of the catalysts.[122] More work is needed to continue to refine our understanding of the basic steps in the kinetic mechanism.
- How many active sites we need to consider in the ZN catalyst? This is a key question to which we do not yet have an answer. Different methods have been proposed over the years to measure the active sites in both unsupported and supported catalysts. One thing is at least certain: it is highly unlikely that all the transition metal atoms in a catalyst formulation are active in polymerization.[123] As the activation of the catalyst sites is a complex process, it is necessary to first identify the number of potential sites on the catalyst surface[124,125] (perhaps more straightforward for a Metallocene than for a ZN catalyst), then attempting to understand how the potential sites are converted to active sites.[126] Significant hope to answering this (and the following) question can eventually be found with tools like molecular modelling.[127]
- How many families of active sites do we have? Again, an obvious but difficult to answer question. Clearly this will be a function of catalyst formulation and thus different for different catalytic systems. Ideally, we would like to know this number *a priori*. Deconvolution methods[128] are commonly used to estimate the ***minimum number*** of families of sites and their associated rate constants based on e.g., high temperature size exclusion chromatography (HT-SEC), eventually coupled with a different chromatographic technique (e.g. TREF, CRYSTAF or CEF) for copolymers. This information is useful for a given catalyst in a given recipe and allows us to model the impact of a process on the MWD or CCD, but at the end of

the day, remains empirical and is not really a guarantee that we have the exact number of site types. There is no reason that this number cannot vary during the course of the polymerization, or that the nature of the active sites must remain constant. Furthermore, one could also ask if different types of sites are more, or less sensitive to poisons?

- How can we estimate these kinetic parameters accurately to match experimental data or industrial processes, without imposing a bias from poorly identified physical phenomena (e.g. poor sorption estimates)? How do these parameters evolve with temperature and time? Although we can find values of kinetic parameters for the common olefin polymerizations in the open literature, it should be kept in mind that these parameters are not universal but are system-dependent.[61] They are specific for the used catalyst/cocatalyst and working temperature. In addition, it is also via questions like these where the micro- and mesoscales are strongly connected. In order to use experimental (or even computational) methods to estimate parameters using the methods mentioned above, one needs to know the values of the concentration of species at the active sites. This implies that we can calculate the solubilities of different species in multicomponent mixtures. We also need to know the characteristic length scale for diffusion (i.e. the particle morphology), as well as the diffusivities of the different species. Solubility and diffusivity depend obviously on the chemical species involved, their bulk concentrations and the local temperature. They also appear to depend on the crystallinity[129] and eventually the molecular weight distribution (at least for LLDPE) of the polymer phase.[107] Care must be taken, in particular if we need to precisely model quantities such as the MWD or CCD to avoid "biasing" true parameter values with poor estimates of thermodynamic properties.

Given these challenges, we propose to attempt to simplify the kinetic model in so far as it is possible. How this is done can depend on the goals of the model (see comment about complexity at the beginning of this section). One of the least clear points in the list above is the number of families of sites needed for a given model. Indeed, the larger the number of active sites in the kinetic model, the longer the computational time for the simulations and it becomes more difficult to identify them based on available data.[61] There are three practical ways used to reduce the number of the kinetic constants in the ZN olefin polymerization system:

(1) Simplified kinetic schemes using a minimum number of elementary reactions (i.e. site activation, chain initiation, chain propagation, chain transfer by hydrogen, dormant site formation and reactivation, and chain termination), while the kinetic model should offer accurate prediction of the overall polymerization rate and polymer average molecular weight.[11] This can be done if some reactions are very fast or very slow (e.g. assume instantaneous catalyst activation, negligible deactivation during its residence time, etc.).
(2) Single-site kinetic model;[17,43,45,46,130] the multiple active sites of the ZN catalyst are lumped together into a single active site. This approach may offer a good prediction of the polymerization rate and polymer MWD if the difference between the activity of the different sites is small, otherwise it cannot be used[61].
(3) Two-lumped active site model; the multiple active sites of the ZN catalyst are lumped into two distinct lumped active sites. This may allow a good prediction of the polymerization rate and average molecular weights in many cases.[131]

Nevertheless, a compromise between the simplicity and the accuracy of the kinetic model should be made to satisfy modelling objectives (i.e. high degree of accuracy prediction of the overall polymerizations rate and polymer average molecular weight).

4.1.2 Polymer properties

While we have a reasonably clear idea how to predict properties such as the MWD and CCD if reasonable kinetic parameters and thermodynamic data are available, the conformation of the chains, and in particular the rate of chain crystallization during the reaction remains poorly understood. In the specific case of gas phase propylene polymerization this issue might be of secondary interest (it appears to be more important in PE processes, but that is a topic for a separate publication). Nevertheless, it is possible that the rate at which the polymer crystallizes can be influenced by the local temperature and how the polymer is swollen during polymerization by the different species present in the continuous phase. It is postulated that the relative rates of chain crystallization and of local polymer production can have an impact on the fragmentation and particle growth stages,[77,88] further tying the microscale to mesoscale events.

4.2 Mesoscale

4.2.1 Thermodynamics

Needless to say, the accuracy of the kinetic model is strongly influenced by the prediction of the thermodynamic and physical properties of the polymerization system.[132] As was discussed above, the accurate estimation of concentrations of the reactive components at the active is a challenging task. As it was seen in Section 3.3.2, both the SL and PC-SAFT EoS models used to calculate the equilibrium sorption requires adjustable interaction parameters (k_{ij}), the values of which are limited to the experimental range used for data fitting, as well as to the specific polymer used in the study. More work is needed to establish a data base for the interaction parameters for a range of penetrant compositions, pressures, temperatures, and eventually macromolecular structure. Concerning the last point, one would expect this is more important for different types of PE than for PP because of the different crystalline structures of the two families of polymers. Nevertheless, information on this important point is scarce.

4.2.2 Transfer limitations at the particle level

Mass and heat transfer limitations are observed at the particle level, and the extent to which these are important might have a large impact on the concentration of different species at the active sites, and therefore on the polymerization rate and polymer properties.[12] Several of the points mentioned in the preceding paragraphs can influence the extent to which these transport rates can be limited, but the one that is the most important of all is the hardest to quantify: the morphology. Several review articles cited above show the problems associated with trying to predict particle morphology *a priori*. An interesting series of papers[133–137] showed that the morphology of a particle will depend on the mechanical properties of the polymer, the rate at which the polymer is produced, and of course the starting point for the catalyst morphology. Therefore, we know that these issues are important but it is still very difficult to predict how the morphology evolves. Without this knowledge, it is not possible to know the particle porosity, nor the characteristic length scales for mass transfer inside the particles.

For these reasons, many (over)simplified assumptions are usually made to allow one to solve the coupled mass and energy balances in the SPM, including:

(1) The shape of the catalyst and polymer particles are often assumed to be spherical, with uniform porosity;

(2) In a link to the macroscale, phenomena such as particle sintering or particle break-up are very poorly understood in terms of our ability to model them [19]. We are well aware that these issues can cause significant problems at the production level, yet aside from some empirical fixes, we do not know how to predict the occurrence of either event as a function of operating conditions, catalyst type, polymer type; etc. In terms of particle agglomeration these particle-particle interactions are strongly influenced by the properties of the polymer particles, and especially by very poorly studied phenomena such as sorption of monomer, comonomer and compounds;

(3) In a related area, static electricity is a very important issue in industrial production, yet very little information is available on this phenomenon as well;

(4) In the estimation of the effective (or overall) diffusivity ("$D_{i,\mathrm{eff}}$" in Equation (33), the change of the particle porosity during the polymerization is neglected (it usually assumes an average porosity instead of using the porosity as a function of reaction time). However, it is now known that the development of the particle structure, particularly in the early stage of polymerization presents a non-negligible porosity variation;[77]

(5) For the energy balances on the particle, the estimation of the external heat transfer coefficient ("h" in Equation (28)) at the particle boundary layer in the gas-phase catalytic olefin polymerization is a major challenge. Several researchers generally employ the traditional Ranz-Marshall correlations together with Nusselt number relationships to determine such coefficient due to their simplicity and ease of use [12]. However, this correlation was originally developed for an isolated and falling droplet, whereas the evolution of the particles in a polymerization reactor are far from isolated[12]. As a result, this correlation significantly underestimated the value of the heat-transfer coefficient, and the prediction of the particle temperature is incorrectly overestimated [83]. It was recently suggested by Kanellopoulos et al.[83] that the modified correlation proposed by Nicolella et al.[138] expressing the Reynolds number in terms of the appropriate energy dissipation rate provides a better estimation for the heat transfer coefficient than the traditional Ranz–Marshall correlation.

The major challenges to joining the micro- and macro-scales in a unified continuity are to be found at the mesoscale. As we just stated, the reasons for this are numerous, but often involve the complexity of the models needed at the mesoscale and a glaring lack of data.

Industrial problems that remain to be solved often revolve around the interactions between particles.

4.3 Macroscale

The modelling of the macroscale can also present a certain number of challenges that need to be resolved, in particular looking at how best to integrate high levels of detail in the final product. In a true multiscale approach, our process model would contain contributions from models at each length scale we choose to include. In a full modelling effort this would necessarily pass by a population balance modelling (PBM) approach. This implies that we keep track of at least different classes of particles, defined for example by their size and their age. We would use an SPM to link the microscale model to the mesoscale and bulk conditions, and then the RTD model to describe the impact of the RTD on the evolution of the said particles. To say the least, this can be a very time-consuming effort (in terms of computational times).

The RTD can be described using different approaches, in particular by the compartmentalized approaches mentioned above. The limiting factor here is that this does not truly allow one to take into consideration the hydrodynamics of the bed and makes it very difficult to predict real challenges such as partial defluidization, flow segregation, the impact of any agglomerates formed (assuming we can use an agglomeration kernel in a PBM to predict their formation), etc. Furthermore, this type of macroscale model relies on time-averaged properties, and at the current time do not allow for randomly occurring events or mesoscale phenomena that can lead to a loss of bed stability.

Computation Fluid Dynamics (CFD) modelling is an attractive response to this shortcoming; at least in principle. Ideally, CFD which offers the ability to precisely model reactor hydrodynamics under a range of operating conditions, particle sizes and continuous phase compositions would be a very powerful tool. While CFD models have the potential for significantly improving our understanding of the hydrodynamics of FBRs, the computational effort required to achieve a useful level of detail is immense.

5 CONCLUSIONS

In this review paper, the recent development on gas-phase catalytic propylene (co)polymerization processes, and multiscale modelling framework in multizone polymerization reactors have been presented. The important aspects including the current issues

and challenges for the development of multiscale modelling at different levels have been highlighted.

This review has shown that the advanced multiscale modelling methodology has provided very useful insights for a deep understanding of how the polymerization kinetics at the active sites, the transport phenomena and thermodynamics at the particle level, and the reactor configurations influence the final product properties such as molecular structure of polymers. A fundamental knowledge of polymer reaction engineering obtained from the multiscale modelling framework allows researchers and engineers to improve the existing models or to develop more refined models to control polymer structures and properties.

However, the development of a complete multiscale model for a commercial reactor is very challenging. Moreover, the solubility and diffusivity data of ternary and higher order polyolefin systems at industrial conditions are very limited in open literature. Without such data, it is difficult to develop the more refined (or complete) models.

6 ACKNOWLEDGEMENT

The authors are grateful to SCG Chemicals Co., Ltd. for technical and financial support of this work.

7 NOTATION

List of Abbreviations

A	Propylene
B	Ethylene
C_3	Propylene
C_2	Ethylene
Cat	Catalyst
Co	Cocatalyst
CCD	Chemical composition distribution
CEF	Crystallization Elution Fractionation
CFD	Computational fluid dynamics
CRYSTAF	Crystallization Analysis Fractionation
CTA	Chain transfer agent
DSC	Differential scanning calorimetry
CSTR	Continuous stirred tank reactor

EPR	Ethylene propylene rubber
FBR	Fluidized bed reactor
FBR-IC	Fluidized bed reactor with internal circulation
FBR-EC	Fluidized bed reactor with external circulation
H_2	Hydrogen
HPPs	Polypropylene homopolymers
HSBR	Horizontal stirred bed reactors
HT-SEC	High temperature size exclusion chromatography
hiPP	High impact polypropylene
ICA	Induced condensing agent
ICP	Impact Polypropylene Copolymer
LLDPE	Linear low-density polyethylene
iPP	Isotactic polypropylene
M	Metallocene catalyst
MGM	Multigrain model
MI	Melt index
$MgCl_2$	Magnesium chloride
$\bar{M}_n$	Average number molecular weights
$\bar{M}_w$	Average weight molecular weights
MWD	Molecular weight distribution
MZCR	Multizone circulating reactor
Nu	Nusselt number
PBM	Population balance modelling
PC-SAFT	Perturbed-chain statistical associating fluid theory
PE	Polyethylene
PFR	Plug flow reactor
PFM	Polymeric flow model
PMLM	Polymeric multilayer model
PP	Polypropylene
PSD	Particle Size Distribution
RCP	Polypropylene random copolymers
Re	Reynolds number
RPPFM	Random pore polymeric flow model

RTD	Residence time distribution
SAFT-EoS	Statistical Associating Fluid Theory Equation of States Model
SL-EoS	Sanchez–Lacombe Equation of State Model
Ti	Titanium atom
$TiCl_3$	Titanium(III) chloride
$TiCl_4$	Titanium tetrachloride
TREF	Temperature Rising Elution Fractionation
XRD	X-ray diffraction
VSBR	Vertical stirred bed reactors
ZN	Ziegler–Natta catalyst

Nomenclature

A	Cross sectional area (m^2)
C_D	Drag coefficient (-)
C_i	Concentration of gas *i* ($mol\ m^{-3}$)
$C_{i,\mathrm{eff}}$	Overall effective concentration of gas *i* per volume of entire pseudo-homogenous particle ($mol\ m^{-3}$)
C^*	Total concentration of active in the catalyst particles ($mol\ m^{-3}$)
C_i^{p}	Concentration of gas *i* in the amorphous polymer phase ($mol\ m^{-3}$)
C_j	Concentration of solid species ($mol\ m^{-3}_{bed}$)
$C_{p,i}$	Heat capacity of the component *i* ($J\ kg^{-1}\ K^{-1}$)
$D_{i,\mathrm{eff}}$	Overall effective diffusivity of the monomer in the semicrystaline polymer phase ($m^2\ s^{-1}$)
D_i^{g}	Gas-phase binary diffusivity of the i^{th} species in a multicomponent gaseous system ($m^2\ s^{-1}$)
D_i^{pol}	Diffusivity of the i^{th} species in the amorphous polymer phase($m^2\ s^{-1}$)
$\bar{d}_{\mathrm{p}}$	Average particle size (m)
d_{r}	Diameter of the reactor (m)
$D_{n,i}$	Concentration of dead polymer chains with length n, terminated with monomer *i* ($mol\ m^{-3}$)
Ea	Activation energy for the reaction ($J\ mol^{-1}$)
$E(t)$	Exit age distribution functions (s^{-1})

F	Mass flow rate (kg s^{-1}) or throughput in the reactor (kg s^{-1}
F^r	Friction losses (kg m^{-2} s^{-1})
g	Acceleration of gravity (m s^{-2})
G	Volumetric growth rate (m^3 s^{-1})
ΔH_{rxn}	Heat of polymerization (J kg^{-1})
h	Heat transfer coefficient (J m^{-2} K^{-1} s^{-1})
h_{D}	Height of the downer (on the bottom of the downer) (m)
h_{R}	Height of the riser (on the top of the riser) (m)
k_0	Pre-exponential factor (m^3 $mol^{-1}s^{-1}$ for 2nd order rate constant; or s^{-1} for 1st order rate constant)
k_{a}	Rate constant of activation by cocatalyst (m^3 mol^{-1} s^{-1})
k_c	Effective thermal conductivity of the particle (J m^{-1} K^{-1} s^{-1})
k_{ij}	Binary interaction parameter between component i and j
$k_{\mathrm{i}j}$	Rate constant for initiation with monomer *j* (m^3 mol^{-1} s^{-1})
$k_{\mathrm{p}ij}$	Rate constant for propagation between active site of type *i* (ending with monomer *i*) and monomer *j* (m^3 mol^{-1} s^{-1})
$k_{\mathrm{tH},j}$	Rate constant for chain transfer of active sites of type *j* to hydrogen ($m^{3/2}$ $mol^{-1/2}$ s^{-1})
$k_{\mathrm{d},j}$	Rate constant of spontaneous deactivation of active site of type *j* (s^{-1})
$k_{\mathrm{d,T}}$	Rate constant of thermal deactivation of a vacant site (m^3 mol^{-1} s^{-1})
$k_{\mathrm{dor},j}$	Rate constant of dormant site formation to a live polymer chain of type *j* (m^3 mol^{-1} s^{-1})
k_{rH}	Rate constant of dormant site reactivation by hydrogen (m^3 mol^{-1} s^{-1})
$K^*_{\mathrm{H}_i}$	Henry constant (mol atm^{-1} L^{-1} amorphous polymer)
L_{r}	Length of the reactor (m)
m	Ratio of the total solids mass hold-up in the HSBR to the number of the CSTRs in series (kg)
$M_{\mathrm{w},i}$	Molecular weight of gas *i* (kg mol^{-1})
N	Total number of CSTRs in series (-)
N_{p}	Number of particles per bed volume (part m^{-3})
P	Pressure (Pa)
P^*	Characteristic pressure (Pa)

P_i	Partial pressure of species *i* (Pa)
$P_{c,i}$	Critical pressure of the monomer *i* (bar)
P_0	Concentration of active vacant sites (mol m^{-3})
P_{0H}	Concentration of active sites with Ti─H bond (mol m^{-3})
$P_{n,i}$	Concentration of living chains of length *n*, terminated with monomer *i* (mol m^{-3})
Q	Volumetric flow rate (m^3 s^{-1})
q_n	Particle density in number per bed volume (part m^{-3} m^{-3}) accounting for the convective flux of particles in the reactor and for the particle growth by polymerization
R	Ideal gas constant (J K^{-1} mol^{-1})
R_{rec}	Recycling ratio (kg kg^{-1})
R_X	Reaction rate of gas species *X* (mol m^{-3} s^{-1})
R_Y	Reaction rate of solid species *Y* (mol m^{-3} s^{-1})
S_p	Concentration of potential active sites (mol m^{-3}_{cat})
$S_{p,d}$	Concentration of deactivated sites (mol m^{-3}_{cat})
S_n	Concentration of dormant sites of length *n* (mol m^{-3}_{solid})
S_r	Reactor cross-section (m^2)
t	Time or residence time (s)
T	Temperature (K)
T^*	Characteristic temperature (K)
$T_{c,i}$	Critical temperature of the monomer *i* (K)
u_g	Gas velocity (m s^{-1})
u_{mf}	Minimum fluidization velocity (m s^{-1})
u_s	Solid velocity (m s^{-1})
u_t	Terminal velocity (m s^{-1})
V	Reactor volume (m^3)
v^*_{mix}	Characteristic closed-packed molar volume of a mer of the mixtures
w_i	Mass fraction of gas *i* in the gas phase (-)
$w_i^{j,in}$	Mass fraction of fresh gas i fed to section j (j = riser or downer)
W	Average molecular weight of monomer species (-)
z	Axial position (m)

Greek letters

γ	Batch polymer yield ($kg_{pol}\,kg^{-1}_{cat}$)
ε	Porosity of the bed (-)
ε^{p}	Porosity of the particle (-)
$\varepsilon^{R,in}$	Porosity at the inlet of the riser (combining fresh feed and outlet of downer)
ε^{*}_{mix}	Characteristic interaction energy for the mixtures
η_k	k^{th} moment of the dormant polymer chains (mol m^{-3})
λ_k	k^{th} moment of the living polymer chains (mol m^{-3})
ρ	Density (kg m^{-3})
ρ^*	Characteristic density (kg m^{-3})
μ	Gas viscosity (kg m^{-1} s^{-1})
μ_k	k^{th} moment of the dead polymer chains (mol m^{-3})
ϕ_p	Volume fraction of polymer (-)
τ	Tortuosity factor (-) or mean residence time (s^{-1})
σ_0^2	Relative variance of the RTD
χ_{pol}	Polymer crystallinity (% wt)

Subscripts or superscripts

A	Annulus section
C	Cone section in FBR-IC
cat	Catalyst
D	Downer
Draft	Draft tube section in FBR-IC
eff	Effective properties
eq	Equilibrium conditions
g	Gas
i	Propylene, Ethylene, H_2, Propane
in	Inlet
k	Number of the employed catalyst active sites
l	Propylene, Ethylene, H_2
L	Length at the boundary layer
lump	Lumped kinetic coefficient

m	Backmixing
n	Index of the CSTR in series (*n* = 1, … , *N*th)
out	Outlet
p	Polymer or particle
prep	Prepolymerization
pol	Polymer
R	Riser
rec	Recycling
s	Solid
tot	Total

8 REFERENCES

[1] J. Karger-Kocsis, T. Bárány, *Polypropylene Handbook*, J. Karger-Kocsis, T. Bárány, Eds., 1st edition, Springer International Publishing, Cham, Switzerland, **2019**.

[2] Fortune Business Insights, "Polypropylene Market Size, Share & Trends | Report [2028]," accessed on December 15, 2021, https://www.fortunebusinessinsights.com/industry-reports/polypropylene-pp-market-101583.

[3] X. Wang, X. Han, R. Xu, "Versatile Propylene-Based Polyolefins with Tunable Molecular Structure through Tailor-Made Catalysts and Polymerization Process," *Polypropylene - Polymerization and Characterization of Mechanical and Thermal Properties*, IntechOpen **2020**.

[4] N. Pasquini, A. Addeo, *Polypropylene Handbook*, N. Pasquini, A. Addeo, Eds., 2nd, illustr edition, Hanser, **2005**.

[5] Hisham A. Maddah, *Am. J. Polym. Sci.* **2016**, *6*, 1.

[6] J. B. P. Soares, T. McKenna, C. P. Cheng, "Coordination Polymerization," *Polymer Reaction Engineering*, J. M. Asua, Ed., Blackwell Publishing Ltd, Oxford, UK **2007**, p. 29.

[7] J. B. P. Soares, T. F. L. McKenna, *Polyolefin Reaction Engineering*, J. B. P. Soares, T. F. L. McKenna, Eds., Wiley-VCH Verlag & Co. KGaA, Weinheim, Germany, **2012**.

[8] V. Kanellopoulos, C. Kiparissides, "Industrial multimodal processes," *Multimodal Polymers with Supported Catalysts: Design and Production*, A. R. Albunia, F. Prades, D. Jeremic, Eds., 1st edition, Springer International Publishing, Cham, Switzerland

2019, p. 155.

[9] T. Xie, K. B. McAuley, J. C. C. Hsu, D. W. Bacon, *Ind. Eng. Chem. Res.* **1994**, *33*, 449.

[10] W. H. Ray, *Berichte der Bunsengesellschaft für Phys. Chemie* **1986**, *90,* 947.

[11] V. Touloupidis, *Macromol. React. Eng.* **2014**, *8*, 508.

[12] T. F. L. McKenna, M. A. Bashir, "Fragmentation, particle growth and single particle modelling," *Multimodal Polymers with Supported Catalysts: Design and Production*, A. R. Albunia, F. Prades, D. Jeremic, Eds., Springer International Publishing, Cham, Switzerland **2019**, p. 81.

[13] W. H. Ray, *Can. J. Chem. Eng.* **1991**, *69*, 626.

[14] C. Kiparissides, *Chem. Eng. Sci.* **1996**, *51*, 1637.

[15] G. Dompazis, V. Kanellopoulos, C. Kiparissides, *Macromol. Mater. Eng.* **2005**, *290*, 525.

[16] J. L. S. Rodriguez, Modelado de la polimerización de olefinas con catalizadores soportados, Universidad del País Vasco-Euskal Herriko Unibertsitatea (Spain), **2002**.

[17] J. L. Santos, J. M. Asua, J. C. De La Cal, *Ind. Eng. Chem. Res.* **2006**, *45*, 3081.

[18] G. Dompazis, V. Kanellopoulos, V. Touloupides, C. Kiparissides, *Chem. Eng. Sci.* **2008**, *63*, 4735.

[19] R. F. Alves, T. Casalini, G. Storti, T. F. L. McKenna, *Macromol. React. Eng.* **2021**, *15*.

[20] J. B. P. Soares, T. F. L. McKenna, "Polyolefin Reactors and Processes," *Polyolefin Reaction Engineering*, J. B. P. Soares, T. F. L. McKenna, Eds., Wiley-VCH Verlag & Co. KGaA, Weinheim, Germany **2012**, p. 87.

[21] P. Galli, G. Vecellio, *Prog. Polym. Sci.* **2001**, *26*, 1287.

[22] B. Liu, B. Liu, J. B. P. Soares, *Macromol. React. Eng.* **2018**, *12*, 1.

[23] C. Grein, "Multimodal polypropylenes: The close interplay between catalysts, processes and polymer design," *Multimodal Polymers with Supported Catalysts: Design and Production*, A. R. Albunia, F. Prades, D. Jeremic, Eds., Springer International Publishing, Cham, Switzerland **2019**, p. 205.

[24] H. Sato, H. Ogawa, Review on Development of Polypropylene Manufacturing, **2009**.

[25] B. Tabiś, A. Essekkat, *Chem. Eng. Sci.* **1992**, *47*, 407.

[26] H. Hatzantonis, H. Yiannoulakis, A. Yiagopoulos, C. Kiparissides, *Chem. Eng. Sci.* **2000**, *55*, 3237.

[27] F. A. N. Fernandes, L. M. F. Lona, *Chem. Eng. Sci.* **2001**, *56*, 963.

[28] R. F. Alves, T. F. L. McKenna, *Ind. Eng. Chem. Res.* **2021**, *60*, 11977.

[29] M. Covezzi, G. Mei, *Chem. Eng. Sci.* **2001**, *56*, 4059.

[30] M. Dorini, G. Mei, "Basell Spherizone Technology," *Sustainable Industrial Chemistry*, F. Cavani, G. Centi, S. Perathoner, F. Trifiró, Eds., Wiley-VCH Verlag GmbH & Co. KGaA, Weinheim, Germany **2009**, p. 563.

[31] WO2004/033505 A1 (**2004**), invs.: Massimo Covezzi, Gerben MEIER, Gabriele Mei.

[32] US 6,689,845 B1 (**2004**), invs.: Gabriele Govoni, Massimo Covezzi.

[33] G. Weickert, "New reactor concepts for gas phase olefin polymerization," 8th International Workshop on Polymer Reaction Engineering, Wiley-VCH Verlag, Weinheim, Germany, **2005**.

[34] G. B. Meier, G. Weickert, W. P. M. van Swaaij, *AIChE J.* **2002**, *48*, 1268.

[35] WO 02/40547 A1 (**2002**), invs.: S. M. P. Mutsers, Gunter WEICKERT.

[36] US 2016/0002376 A1 (**2016**), invs.: Sung Woo KANG, Byung Soon CHUN, Young Jae JUN.

[37] WO / 2000/069552 (**2000**), invs.: S. M. P. Mutsers.

[38] M. Caracotsios, *Chem. Eng. Sci.* **1992**, *47*, 2591.

[39] C. J. Dittrich, S. M. P. Mutsers, *Chem. Eng. Sci.* **2007**, *62*, 5777.

[40] T. F. L. M. J.B.P. Soares, *Can. J. Chem. Eng.* **2022**.

[41] Y.-P. Zhu, G.-Q. Chen, Z.-H. Luo, *Macromol. React. Eng.* **2014**, *8*, 609.

[42] Zhou Tian Xue-Ping Gu Lian-Fang Feng Jean-Pierre Corriou Guo-Hua, *J. Appl. Polym. Sci.* **2011**, *125*, 2668.

[43] F. A. N. Fernandas, L. M. F. Lona, *J. Appl. Polym. Sci.* **2004**, *93*, 1042.

[44] F. A. N. Fernandas, L. M. F. Lona, *J. Appl. Polym. Sci.* **2004**, *93*, 1053.

[45] H. Adli, N. Mostoufi, S. M. Ghafelebashi, *J. Appl. Polym. Sci.* **2011**, *122*, 393.

[46] N. M. Ghasem, W. L. Ang, M. A. Hussain, *Chem. Prod. Process Model.* **2008**, *3*.

[47] N. M. Ghasem, W. L. Ang, M. A. Hussain, *Korean J. Chem. Eng.* **2009**, *26*, 603.

[48] G. B. Meier, G. Weickert, W. P. M. van Swaaij, *J. Polym. Sci. Part A Polym. Chem.* **2001**, *39*, 500.

[49] J. J. Zacca, J. A. Debling, W. H. Ray, *Chem. Eng. Sci.* **1996**, *51*, 4859.

[50] N. P. Khare, B. Lucas, K. C. Seavey, Y. A. Liu, A. Sirohi, S. Ramanathan, S. Lingard, Y. Song, C.-C. Chen, *Ind. Eng. Chem. Res.* **2004**, *43*, 884.

[51] J. B. P. Soares, A. E. Hamielec, *Polymer (Guildf).* **1996**, *37*, 4607.

[52] J. J. Zacca, J. A. Debling, W. H. Ray, *Chem. Eng. Sci.* **1997**, *52*, 1941.

[53] J. A. Debling, J. J. Zacca, W. H. Ray, *Chem. Eng. Sci.* **1997**, *52*, 1969.

[54] J. A. Debling, W. Harmon Ray, *J. Appl. Polym. Sci.* **2001**, *81*, 3085.

[55] A. Shamiri, M. A. Hussain, F. S. Mjalli, M. S. Shafeeyan, N. Mostoufi, *Ind. Eng. Chem. Res.* **2014**, *53*, 8694.

[56] G. H. Varshouee, A. Heydarinasab, A. Vaziri, S. M. G. Zarand, *Kem. Ind.* **2019**, *68*, 269.

[57] N. Sharma, Y. A. Liu, *Ind. Eng. Chem. Res.* **2019**, *58*, 14209.

[58] N. P. Khare, PREDICTIVE MODELING OF METAL-CATALYZED POLYOLEFIN PROCESSES, Virginia Polytechnic Institute and State University, **2003**.

[59] V. Touloupidis, G. Rittenschober, C. Paulik, *Macromol. React. Eng.* **2020**, *14*, 1.

[60] A. Zecchina, S. Bordiga, E. Groppo, "The Structure and Reactivity of Single and Multiple Sites on Heterogeneous and Homogeneous Catalysts: Analogies, Differences, and Challenges for Characterization Methods," *Selective Nanocatalysts and Nanoscience: Concepts for Heterogeneous and Homogeneous Catalysis*, A. Zecchina, S. Bordiga, E. Groppo, Eds., Wiley-VCH Verlag GmbH & Co. KGaA, Weinheim, Germany **2011**, p. 1.

[61] A. K. Thakur, S. K. Gupta, P. Chaudhari, *Rev. Chem. Eng.* **2020**.

[62] K. Czaja, M. BiaŁek, *J. Appl. Polym. Sci.* **2001**, *79*, 361.

[63] A. Alizadeh, M. Namkajorn, E. Somsook, T. F. L. McKenna, *Macromol. Chem. Phys.* **2015**, *216*, 985.

[64] Y. V. Kissin, R. I. Mink, T. E. Nowlin, *J. Polym. Sci. Part A Polym. Chem.* **1999**, *37*, 4255.

[65] M. A. Ali, B. Betlem, B. Roffel, G. Weickert, *AIChE J.* **2006**, *52*, 1866.

[66] G. H. Varshouee, A. Heydarinasab, U. Shaheen, M. A. S. Aborehab, A. Vaziri, Y. El Ouadi, B. Roozbahani, A. Bouyanzer, B. Hammouti, T. Ben Hadda, Hydrogen effect modeling on Ziegler-Natta catalyst and final product properties in propylene polymerization, **2018**, https://www.ajol.info/index.php/bcse/article/view/174941.

[67] I. C. van Putten, M. van Sint Annaland, G. Weickert, *Chem. Eng. Sci.* **2007**, *62*, 2522.

[68] I. C. van Putten, Propylene polymerization in a circulating slugging fluidized bed reactor, University of Twente, **2004**.

[69] J. Soares, *Chem. Eng. Sci.* **2001**, *56*, 4131.

[70] M. A. Dubé, J. B. P. Scares, A. Penlidis, A. E. Hamielec, *Ind. Eng. Chem. Res.* **1997**, *36*, 966.

[71] J. Kettner, *Kinetic investigation of different supported catalysts for the polymerization of propylene under industrially relevant conditions*, Cuvillier, Germany, **2019**.

[72] V. Matos, M. Moreira, A. G. M. Neto, M. Nele, P. A. Melo, J. C. Pinto, *Macromol. React. Eng.* **2007**, *1*, 137.

[73] K. Chen, S. Mehdiabadi, B. Liu, J. B. P Soares, K. Chen, S. Mehdiabadi, J. B. P Soares, B. Liu, *Wiley Online Libr.* **2016**, *10*, 551.

[74] J. B. P. Soares, T. F. L. McKenna, "Particle Growth and Single Particle Modeling," *Polyolefin Reaction Engineering*, J. B. P. Soares, T. F. L. McKenna, Eds., Wiley-VCH Verlag GmbH & Co. KGaA, Weinheim, Germany **2012**, p. 271.

[75] S. Floyd, K. Y. Choi, T. W. Taylor, W. H. Ray, *J. Appl. Polym. Sci.* **1986**, *32*, 2935.

[76] R. Alves, M. A. Bashir, T. F. L. McKenna, *Ind. Eng. Chem. Res.* **2017**, *56*, 13582.

[77] A. Alizadeh, T. F. L. McKenna, *Macromol. React. Eng.* **2018**, *12*, 1700027.

[78] W. R. Schmeal, J. R. Street, *AIChE J.* **1971**, *17*, 1188.

[79] W. R. Schmeal, J. R. Street, *J. Polym. Sci. Polym. Phys. Ed.* **1972**, *10*, 2173.

[80] R. Galvan, M. Tirrell, *Chem. Eng. Sci.* **1986**, *41*, 2385.

[81] R. Galvan, M. Tirrell, *Comput. Chem. Eng.* **1986**, *10*, 77.

[82] V. Kanellopoulos, E. Tsiliopoulou, G. Dompazis, V. Touloupides, C. Kiparissides, *Ind. Eng. Chem. Res.* **2007**, *46*, 1928.

[83] V. Kanellopoulos, G. Dompazis, B. Gustafsson, C. Kiparissides, *Ind. Eng. Chem. Res.* **2004**, *43*, 5166.

[84] R. A. Hutchinson, C. M. Chen, W. H. Ray, *J. Appl. Polym. Sci.* **1992**, *44*, 1389.

[85] J. A. Debling, W. H. Ray, *Ind. Eng. Chem. Res.* **1995**, *34*, 3466.

[86] T. F. McKenna, J. B. P. Soares, *Chem. Eng. Sci.* **2001**, *56*, 3931.

[87] A. Ben Mrad, N. Sheibat-Othman, T. F. L. McKenna, *Macromol. React. Eng.* **2021**, *2100016*, 1.

[88] T. F. L. McKenna, A. Di Martino, G. Weickert, J. B. P. Soares, *Macromol. React. Eng.* **2010**, *4*, 40.

[89] S. A. Stern, J. T. Mullhaupt, P. J. Gareis, *AIChE J.* **1969**, *15*, 64.

[90] R. A. Hutchinson, W. H. Ray, *J. Appl. Polym. Sci.* **1990**, *41*, 51.

[91] A. J. Cancelas, M. A. Plata, M. A. Bashir, M. Bartke, V. Monteil, T. F. L. McKenna, *Macromol. Chem. Phys.* **2018**, *219*, 1.

[92] W. G. Chapman, K. E. Gubbins, G. Jackson, M. Radosz, *Fluid Phase Equilib.* **1989**, *52*, 31.

[93] N. Pedrosa, L. F. Vega, J. A. P. Coutinho, I. M. Marrucho, *Macromolecules* **2006**, *39*, 4240.

[94] J. Gross, G. Sadowski, *Ind. Eng. Chem. Res.* **2001**, *40*, 1244.

[95] G. Sadowski, "Modeling of polymer phase equilibria using equations of state," *Advances in Polymer Science,Polymer Thermodynamics*, S. Enders, B. A. Wolf, Eds., Springer, Berlin, Heidelberg, Berlin, Germany **2010**, p. 389.

[96] J. Gross, O. Spuhl, F. Tumakaka, G. Sadowski, *Ind. Eng. Chem. Res.* **2003**, *42*, 1266.

[97] I. C. Sanchez, R. H. Lacombe, *J. Phys. Chem.* **1976**, *80*, 2352.

[98] R. H. Lacombe, I. C. Sanchez, *J. Phys. Chem.* **1976**, *80*, 2568.

[99] A. Krallis, V. Kanellopoulos, *Ind. Eng. Chem. Res.* **2013**, *52*, 9060.

[100] A. Alizadeh, J. Chmelař, F. Sharif, M. Ebrahimi, J. Kosek, T. F. L. McKenna, *Ind. Eng. Chem. Res.* **2017**, *56*, 1168.

[101] A. Alizadeh, Study of Sorption, Heat and Mass Transfer during Condensed Mode Operation of Gas Phase Ethylene Polymerization on Supported Catalyst, UNIVERSITE CLAUDE BERNARD - LYON 1, **2014**.

[102] Y. Sato, A. Tsuboi, A. Sorakubo, S. Takishima, H. Masuoka, T. Ishikawa, *Fluid Phase Equilib.* **2000**, *170*, 49.

[103] A. Ben Mrad, S. Norsic, N. Sheibat-Othman, T. F. L. McKenna, *Ind. Eng. Chem. Res.* **2021**, *60*, 10791.

[104] R. F. Alves, T. F. L. McKenna, *Chem. Eng. J.* **2020**, *383*, 123114.

[105] A. Novak, M. Bobak, J. Kosek, B. J. Banaszak, D. Lo, T. Widya, W. H. Ray, J. J. de Pablo, *J. Appl. Polym. Sci.* **2006**, *100*, 1124.

[106] E. L. Cussler, "Diffusion Coefficients and Diffusion of Interacting Species," *Diffusion: Mass Transfer in Fluid Systems*, E. L. Cussler, Ed., 2nd edition, Cambridge University Press, Cambridge **2009**, p. 126.

[107] A. Ben Mrad, N. Sheibat-Othman, S. Valaei, M. Bartke, T. F. L. McKenna, *Macromol. Chem. Phys.* **2021**, 2100406.

[108] K. Y. Choi, W. H. Ray, *Chem. Eng. Sci.* **1985**, *40*, 2261.

[109] A. Mahecha-Botero, J. R. Grace, S. S. E. H. Elnashaie, C. J. Lim, *Chem. Eng. Commun.* **2009**, *196*, 1375.

[110] P. A. Mueller, J. R. Richards, J. P. Congalidis, *Macromol. React. Eng.* **2011**, *5*, 261.

[111] M. F. Atan, M. A. Hussain, M. R. Abbasi, M. J. Hossain Khan, M. F. Abdul Patah, *Processes* **2019**, *7*, 1.

[112] P. Cai, L. Chen, J. Van Egmond, M. Tilston, *Particuology* **2010**, *8*, 578.

[113] A. B. Gorbach, S. D. Naik, W. H. Ray, *Chem. Eng. Sci.* **2000**, *55*, 4461.

[114] L. H. Wei, W. C. Yan, Z. H. Luo, *Powder Technol.* **2011**, *214*, 143.

[115] W. C. Yan, J. Li, Z. H. Luo, *Powder Technol.* **2012**, *231*, 77.

[116] W. C. Yan, G. Q. Chen, Z. H. Luo, *Ind. Eng. Chem. Res.* **2012**, *51*, 15132.

[117] R. Marandi, M. Kamyabi, N. Mostoufi, *Can. J. Chem. Eng.* **2018**, *96*, 670.

[118] A. Haider, O. Levenspiel, *Powder Technol.* **1989**, *58*, 63.

[119] Z. Tian, X.-P. Gu, L.-F. Feng, J.-P. Corriou, G.-H. Hu, *J. Appl. Polym. Sci.* **2012**, *125*, 2668.

[120] I. Kouzai, K. Fukuda, *Macromol. Symp.* **2009**, *285*, 23.

[121] B. Liu, J. Romero, B. Liu, J. B. P. Soares, *Macromol. React. Eng.* **2018**, *12*, 1800051.

[122] A. J. Cancelas, V. Monteil, T. F. L. McKenna, *React. Chem. Eng.* **2017**, *2*, 75.

[123] M. M. Ranieri, J. P. Broyer, F. Cutillo, T. F. L. McKenna, C. Boisson, *Dalt. Trans.* **2013**, *42*, 9049.

[124] A. Piovano, T. Wada, A. Amodio, G. Takasao, T. Ikeda, D. Zhu, M. Terano, P. Chammingkwan, E. Groppo, T. Taniike, *ACS Catal.* **2021**, *11*, 13782.

[125] E. S. Merijn Blaakmeer, F. J. Wensink, E. R. H. Van Eck, G. A. De Wijs, A. P. M. Kentgens, *J. Phys. Chem. C* **2019**, *123*, 14490.

[126] Y. V. Kissin, *J. Catal.* **2012**, *292*, 188.

[127] T. Taniike, M. Terano, *J. Japan Pet. Inst.* **2018**, *61*, 182.

[128] A. A. Alghyamah, J. B. P. Soares, *Macromol. Rapid Commun.* **2009**, *30*, 384.

[129] J. Chmelař, K. Smolná, K. Haškovcová, M. Podivinská, J. Maršálek, J. Kosek, *Polymer (Guildf).* **2015**, *59*, 270.

[130] Z. Yang, H. Peng, W. Wang, T. Liu, *J. Appl. Polym. Sci.* **2010**, *116*, 2658.

[131] F. Gemoets, M. Zhang, T. W. Karjala, B. W. S. Kolthammer, *Macromol. React. Eng.* **2010**, *4*, 109.

[132] C. Kipsrissides, *IFAC Proc. Vol.* **2004**, *37*, 137.

[133] Z. Grof, J. Kosek, M. Marek, P. M. Adler, *AIChE J.* **2003**, *49*, 1002.

[134] B. Horáčková, Z. Grof, J. Kosek, *Chem. Eng. Sci.* **2007**, *62*, 5264.

[135] J. Kosek, F. Stepanek, A. Novak, Z. Grof, M. Marek, *Comput. Aided Chem. Eng.* **2001**, *9*, 177.

[136] Z. Grof, J. Kosek, M. Marek, *Ind. Eng. Chem. Res.* **2005**, *44*, 2389.

[137] Z. Grof, J. Kosek, M. Marek, *AIChE J.* **2005**, *51*, 2048.

[138] C. Nicolella, M. C. M. Van Loosdrecht, J. J. Heijnen, *Chem. Eng. Sci.* **1998**, *53*, 2743.

9 SUPPORTING INFORMATION

The supporting information contains a description of commercial gas phase propylene processes, the Sanchez-Lacobme equation of state, and the calculation of the terminal velocity.